AGU PUBLICATIONS

JGR

Journal of Geophysical Research: Planets

RESEARCH ARTICLE
10.1002/2014JE004720

Key Points:
- The north polar spiral troughs are fundamentally similar with regional diversity
- Troughs formed in two stages: (1) during 600 m of deposition and (2) punctuated
- Three processes for trough evolution: wind, insolation, and deposition

Correspondence to:
I. B. Smith,
isaac@boulder.swri.edu

Citation:
Smith, I. B., and J. W. Holt (2015), Spiral trough diversity on the north pole of Mars, as seen by Shallow Radar (SHARAD), *J. Geophys. Res. Planets*, *120*, doi:10.1002/2014JE004720.

Received 8 SEP 2014
Accepted 16 JAN 2015
Accepted article online 27 JAN 2015

Spiral trough diversity on the north pole of Mars, as seen by Shallow Radar (SHARAD)

Isaac B. Smith[1] and John W. Holt[2]

[1]Southwest Research Institute, Boulder, Colorado, USA, [2]Institute for Geophysics, Jackson School of Geosciences, University of Texas at Austin, Austin, Texas, USA

Abstract We combine observations from ground penetrating radar and optical instruments to conduct a comprehensive survey of spiral troughs on the north polar layered deposits of Mars. Our survey reveals that all north polar troughs have common characteristics, but there is strong regional diversity. We divide the north polar layered deposits (NPLD) into eight regions based on observations of morphology and stratigraphy in order to classify the spiral troughs. Morphologic features that separate the regions include central promontories, topographic undulations, bedrock floors, and trough asymmetry among others. We demonstrate here that the troughs formed during two periods. The first generation of troughs formed on the main lobe and in part of Gemina Lingula during accumulation of ~600 m of ice and dust. The second generation of troughs formed stratigraphically higher and immediately after large-scale erosion in Gemini Scopuli, which we conclude created the slopes necessary for troughs to form. We test scenarios of trough evolution and find that only three concurrent processes are required for their formation: wind transport, insolation-induced sublimation, and atmospheric deposition. Our observations are inconsistent with other hypothesized processes to produce spiral troughs, including incision after the formation of the NPLD, fracturing due to flowing ice, and sublimation-driven patterns from insolation.

1. Introduction

Layers of ice and dust deposited during the Amazonian Period cover the north polar region of Mars (Figure 1) [*Tanaka et al*., 2008]. Studies of exposed stratigraphy in the north polar layered deposits (NPLD) have been conducted for decades attempting to find a record of accumulation [*Cutts and Lewis*, 1982; *Howard et al*., 1982; *Levrard et al*., 2007; *Fishbaugh et al*., 2010; *Hvidberg et al*., 2012]. The NPLD actively exchange moisture with the atmosphere and are fundamentally tied to the global water cycle of Mars [*Laskar et al*., 2002; *Head et al*., 2003]. Therefore, they are widely considered to contain the best record of recent climate in the Amazonian [*Fishbaugh and Hvidberg*, 2006; *Byrne*, 2009]. Many investigations have examined the layers of the NPLD with the goal of extracting the depositional and climatic history associated with ice accumulation. Layers are primarily exposed by extensive spiral troughs and scarps [*Milkovich and Head*, 2005; *Fishbaugh and Hvidberg*, 2006; *Byrne*, 2009].

Recently, radar sounding from the Mars Advanced Radar for Subsurface and Ionospheric Sounding on Mars Express and the Shallow Radar (SHARAD) instrument on Mars Reconnaissance Orbiter (MRO) have provided a new method of looking into the NLPD subsurface [*Picardi et al*., 2005; *Seu et al*., 2007]. SHARAD, in particular, has provided remarkable observations of NPLD stratigraphy, proving invaluable for characterizing the evolution of the NPLD [*Phillips et al*., 2008; *Putzig et al*., 2009; *Holt et al*., 2010]. Based on stratigraphy revealed by SHARAD and on process modeling, *Smith et al*. [2013] determined that local processes affect the layers exposed in the spiral troughs. Specifically, they found that interaction between trough morphology and wind determines how and where ice and dust accumulate. Previous work found that the troughs have been an integral part of NPLD surface evolution since their onset prior to the most recent ~700 m of accumulation [*Smith and Holt*, 2010]. Therefore, a better understanding of trough processes should result in a better understanding of the development of the NPLD.

Here we present the first comprehensive survey of troughs and related features using SHARAD. We analyze stratigraphy, compare to optical data, draw inferences on pertinent observations, and present hypotheses regarding the development of the NPLD with respect to the spiral troughs.

Since individual troughs are not circumpolar features and references to their equator and pole-facing slopes are inadequate, we adopt the reference frame of *Smith et al*. [2013, 2014] concerning high and low sides of

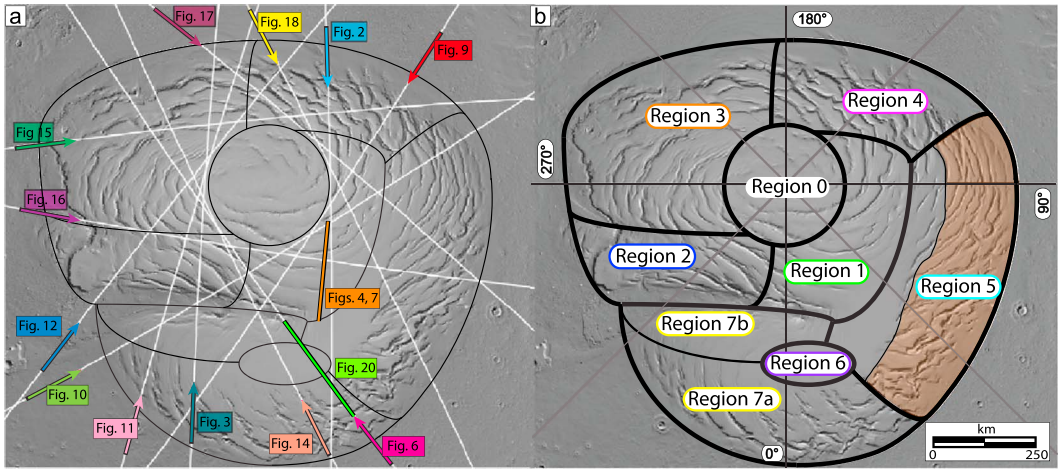

Figure 1. MOLA Hillshade of the NPLD [*Smith et al.*, 2001]. (a) Ground tracks of figures in this paper. (b) NPLD troughs are similar but vary by region. Region 5 erosion extent is highlighted. Colors surrounding each region name correspond to colored bars near the top of figures that contain radargrams.

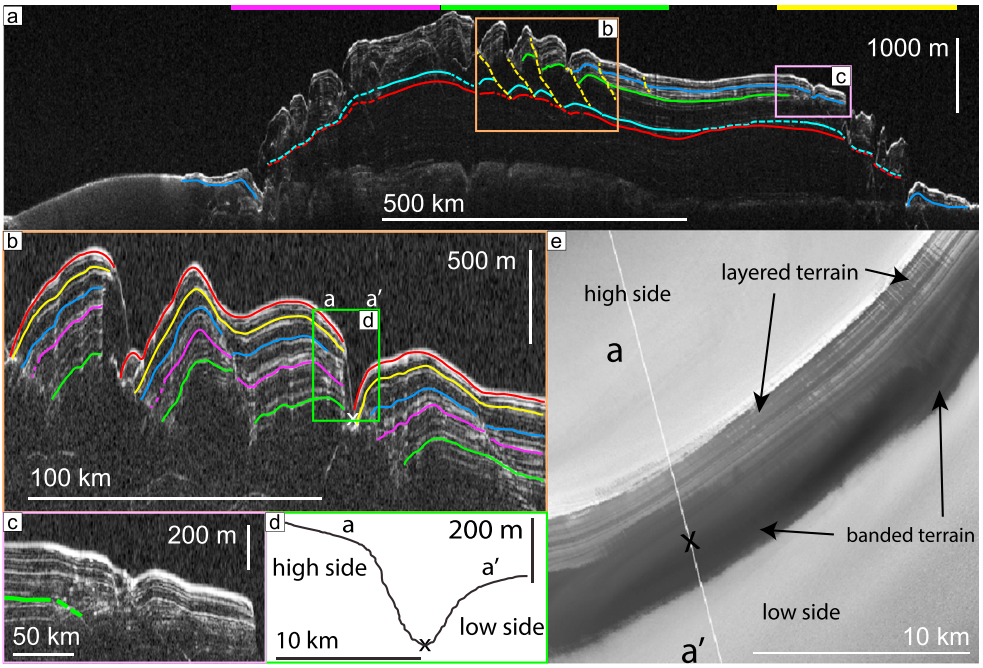

Figure 2. Trough observations. (a) SHARAD observation 1247002 displaying entirety of NPLD. (Location in Figure 1a and colored bars above the NPLD correspond to the regions.) Several horizons are traced throughout the paper: red is Reflector 29 (R29), light blue is Reflector 25 (R25 or trough initiation surface 1, TIS-1), and green is Reflector 17 (R17 or trough initiation surface 2, TIS-2). Reflector names are referenced in Table A1. Yellow dashed lines indicate trough migration paths (TMPs). The three southernmost TMPs identified do not reach R29, indicating that these troughs formed later than many others. Vertical exaggeration (VE) is ~120X. (b) Portion of Figure 2a in Region 1. Individual reflectors are offset at the TMP by as much as 300 m. Layers are thinnest at the trough high-side wall. Layers thicken on the low side. Locations of X, a′, and a″ correspond to the same in Figures 2d and 2e. (c) Portion of Figure 2a displaying a bright reflector and unconformity associated with TIS-2. (d) Topographic profile from MOLA data corresponding to track shown in Figure 2e. Trough sides are asymmetric in slope and elevation. (e) Portion of the Context Imager (CTX) image P01_001595_2665_XN_86N319W. High side exposes fine layers. Wind streaks indicate direction of flow. Black X marks the lowest elevation of the trough. Downwind of the X, on the trough low side, banded terrain overlies layers.

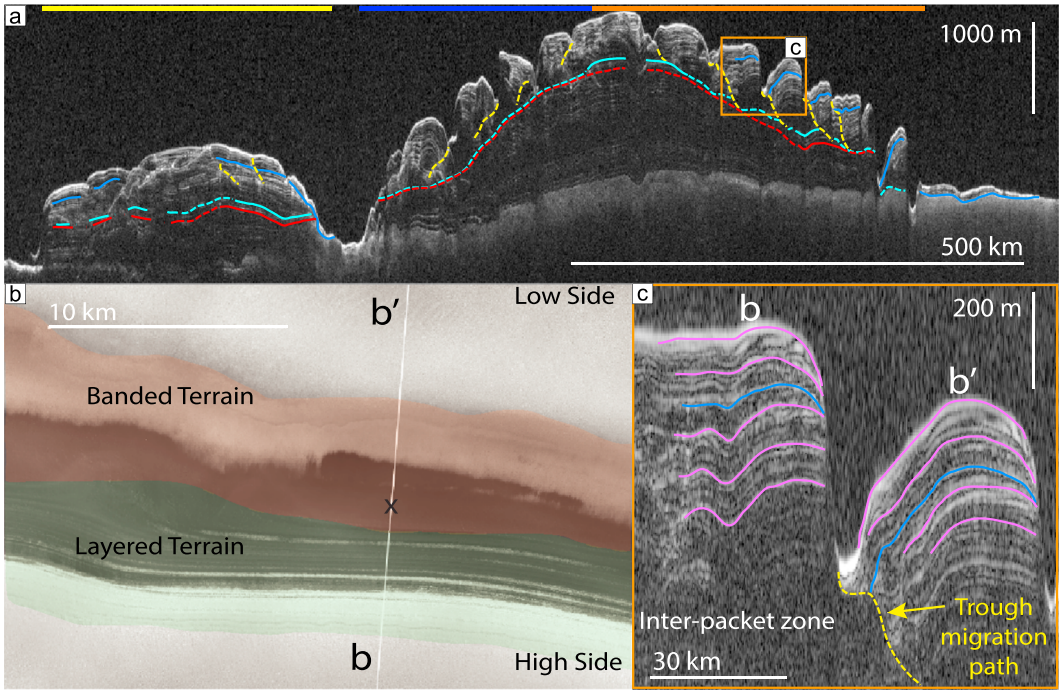

Figure 3. Trough observations. (a) SHARAD observation 2162801. Red and light blue lines trace R29 and R25, respectively, the same as in Figure 2a. VE ~100X. (b) Portion of CTX image P01_001416_ 2665_XI_86N132W displaying layered terrain (green shade) on the high side and banded terrain (orange shade) on the low side. Ground track of Figure 3c in white. Black X is lowest elevation of trough. (c) Portion of Figure 3a in Region 3. Layers are offset by hundreds of meters across the trough and across the TMP. Layers are generally uniform in thickness on the high side of each trough except within the uppermost ~150 m, where they thin, potentially the result of a climatic change. A TMP is easily delimited where low-side layers onlap interpacket material (yellow dashed line). A unit of weak radar reflectors as described by *Putzig et al.* [2009] is found in the lowermost ~100 m of the high side of this trough.

troughs. This classification has the benefit of being independent of trough location and orientation. The high side is topographically higher than the rest of the trough and generally faces toward the equator. The low side is topographically lower and faces generally toward the pole (Figures 2b and 2e).

2. Previous Observations Related to Troughs

Since their discovery in Mariner 9 images [*Murray et al.*, 1972], the NPLD spiral troughs and their stratigraphy have been studied in detail for more than 40 years [*Cutts*, 1973; *Cutts et al.*, 1979; *Squyres*, 1979; *Blasius et al.*, 1982; *Howard et al.*, 1982; *Weijermars*, 1986; *Howard*, 2000; *Tanaka et al.*, 2008; *Smith and Holt*, 2010; *Smith et al.*, 2013, 2014]. The very earliest stratigraphic analyses found that most troughs conform to a few generalizations as follows: asymmetric accumulation of ice across the troughs, exposed layers on the high side, and banded terrain on the low side (Figures 2 and 3) [*Howard et al.*, 1982]. Banded terrain is described as "irregular layering that unconformably overlies adjacent terrain and has an albedo intermediate to the layered and inter-troughs regions." These observations led to an interpretation of poleward migration resulting from erosion on the high side and accumulation on the low side, with an estimated 43–130 m of migration occurring as 10 m of ice accumulated [*Howard et al.*, 1982].

Attempts to provide mechanisms to explain trough formation and gross morphological characteristics were abundant. These studies resulted in hypotheses that varied greatly: nonuniform accumulation [*Cutts et al.*, 1979], Coriolis-oriented fractures from glacial surges [*Weijermars*, 1986; *Zeng et al.*, 2008], local recycling of ice from ablation [*Fisher*, 1993], purely erosional cutting from wind and insolation [*Kolb and Tanaka*, 2001; *Rodriguez and Tanaka*, 2011], lateral heat transfer within the surface [*Pelletier*, 2004], incision due to ablation and then viscous relaxation [*Pathare and Paige*, 2005], and atmospheric deposition of low albedo material causing spatially periodic, spiral sublimation [*Ng and Zuber*, 2006] among others. Each of these models

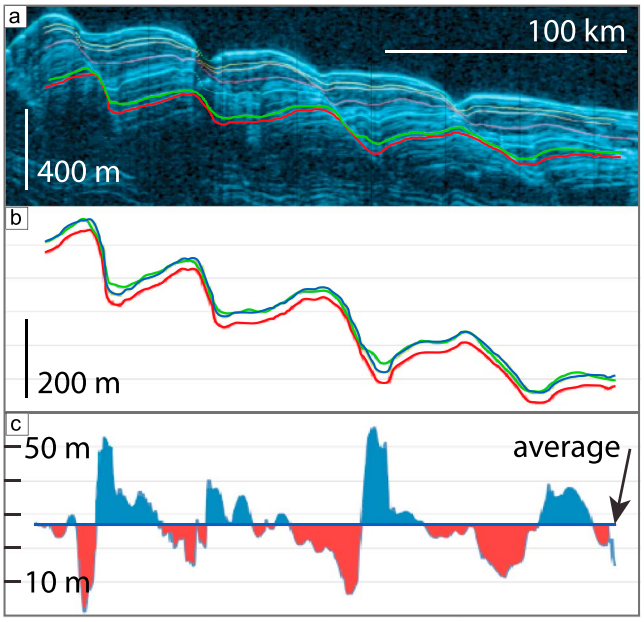

Figure 4. Accumulation patterns in Region 1. (a) SHARAD observation 477002 with interpreted reflectors. (b) Two reflectors (red and green) were chosen to calculate average accumulation over a 240 km stretch of NPLD. The average accumulation of 27 m was added uniformly to the red reflector (blue). (c) Plot of the difference between average (blue in Figure 4b) and measured accumulation (green in Figure 4b): blue is excess or layer thickening, and red is lost ice or layer thinning. The pattern of asymmetric accumulation is readily apparent.

provided a mechanism to form spiral depressions but implied a wide disparity of stratigraphies, none of which agreed with interpretations based on observations of *Howard et al*. [1982] [*Smith et al*., 2013].

Due to the abundance of hypotheses, a test with new instrumentation was necessary. SHARAD, a ground-penetrating radar, is able to probe the NPLD subsurface and is the perfect instrument to test formation hypotheses. However, initial observations were inconclusive. *Phillips et al*. [2008] observed stratigraphic anomalies in the reflections beneath the spiral troughs (Figures 2 and 3) but were unable to determine their nature. *Putzig et al*. [2009] provided the first detailed examination of internal structure of the NPLD but offered no interpretations of trough-related stratigraphy.

A study conducted by *Smith and Holt* [2010] was the first to recognize the stratigraphic anomalies detected by SHARAD as being the result of discontinuous reflectors. They found that the uppermost reflectors within the NPLD are offset vertically across these discontinuities by hundreds of meters (Figures 2b and 3c). Three-dimensional mapping by *Smith and Holt* [2010] demonstrated that the discontinuities were spatially correlated with the spiral troughs, beginning at trough bottoms and extending $>$700 m into the 2000 m thick NPLD. They concluded that the discontinuities were bounding surfaces created during bed form migration, supporting the observations of *Howard et al*. [1982], and called them trough migration paths (TMPs). The troughs migrated 70–115 m during the accumulation of 10 m of ice, consistent with the prediction of *Howard et al*. [1982] but with smaller uncertainties.

Variations in reflection separation (a proxy for layer thickness) were observed in the initial SHARAD trough survey. *Smith and Holt* [2010] found that on either side of the TMP layer thickness varied by distance (Figure 4). Reflectors on the high side decrease in separation (thinner layers) nearer to the TMP, and those on the low side have greater separation (thicker layers) nearer to the TMP (Figures 2 and 4), indicative of transport of ice across the trough [*Howard et al*., 1982; *Smith et al*., 2013].

Based on the thickness variations and TMP mapping, *Smith et al*. [2013] suggested that three largely independent processes determine the slope of the TMP: lateral transfer of ice by wind, insolation-induced sublimation, and atmospheric deposition. High accumulation, low sublimation, or reduced winds cause the TMP slope to increase, while periods of low accumulation, enhanced sublimation, or increased winds cause the slope to decrease (Figure 5). All three factors likely varied through time, yet the stratigraphy would not be preserved without net accumulation.

Topographic undulations are found on the NPLD adjacent to the low side of some spiral troughs [*Howard*, 2000]. Undulations are "wavelike ridges and swales" [*Cutts et al*., 1979] interpreted to be the result of various processes: viscous relaxation of former spiral troughs [*Pathare and Paige*, 2005], remnants of trough migration [*Squyres*, 1979], and ice cap advance and retreat [*Cutts et al*., 1979]. More recently, undulations have been tied to depositional patterns associated with katabatic flow [*Smith et al*., 2013] and are considered analogs to Antarctic megadunes [*Herny et al*., 2014], a form of aeolian antidune [*Dadic et al*., 2013].

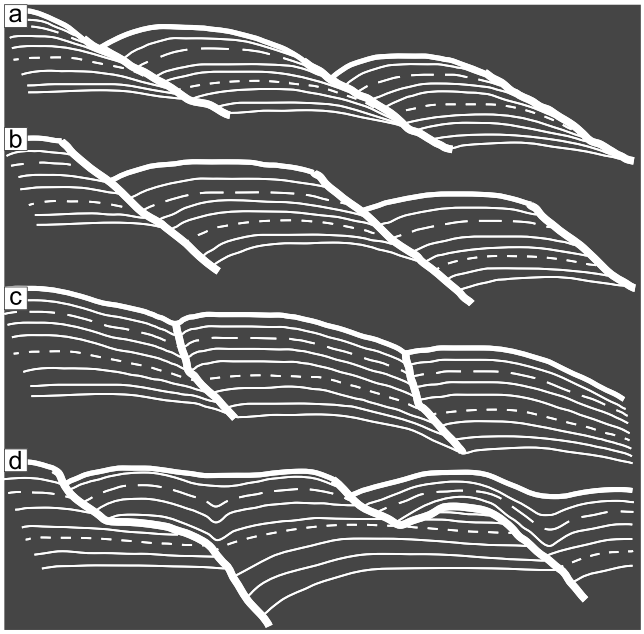

Figure 5. Sketches of trough migration varieties detected in this study. Vertical exaggeration is similar to radargrams shown in other figures. Uniform initial deposition from the atmosphere is assumed unless noted. (a) Migration involving enhanced wind transport. Troughs have thinned layers on the high side of the TMP and thickened layers on the low side. Migration is relatively rapid, and the TMP slope is low, similar to many Region 1 troughs (Figure 4). (b) Reduced wind transport relative to insolation. Individual layers are discontinuous and offset significantly. Layers show some thickening and thinning across the TMP but smaller variation due to reduced transport. TMP is steeper than in Region 1, similar to troughs in Region 3 (Figure 3c). (c) Migration that changes due to increased accumulation, with resulting steepened TMP, similar to some troughs in Regions 1 and 5 (Figure 17c). With enhanced deposition, layers are not eroded, leaving them continuous. (d) Migration over central step (left) and promontory (right). Migration over the promontory is shallow or downward, but continued deposition results in a steepened TMP slope. Concave-up stratigraphy remains.

3. Methods

3.1. SHARAD Data

SHARAD has been operating since late 2006. The instrument is a radar sounder that sends a chirped, 80 μs pulse from 15 to 25 MHz and records reflected energy versus time. Reflections result from contrasts in the real part of the permittivity, ε, which also determines the velocity of the radar waves. Within water ice, SHARAD has a theoretical vertical resolution of ~8.4 m [*Seu et al*., 2007]. Multiple pulses of energy are coherently summed onboard MRO and relayed to Earth for further processing that includes pulse compression, synthetic aperture focusing, and corrections for ionospheric distortion [*Campbell et al*., 2011]. After processing, SHARAD resolves targets down to 0.3–1 km along track and 3–6 km cross track [*Seu et al*., 2007].

Since reaching Mars, approximately 2600 SHARAD observations crossing the NPLD have been collected. Frequent observations at high latitudes provide very tight spatial coverage useful for analysis. With the wealth of data, we utilize both repeated and crossing observations to increase confidence in interpretations. Repeated observations are important for checking against artifacts of processing or low signal strength. By examining from multiple orientations, our view of subsurface geometries is improved, eliminating ambiguous interpretations. Furthermore, observations of a target from multiple orientations help to distinguish surface clutter (see below) from scientifically interesting subsurface reflections.

3.2. Mitigating Clutter

SHARAD has a dipole antenna that radiates in a modified torus. The orbital altitude of ~300 km effectively results in a plane wave that reaches the surface. Surface reflections may return from anywhere in the antenna pattern. Hence, the point directly below the spacecraft, or the nadir point, provides only a portion of the return signal. Typically, surface reflections resulting from locations far away from nadir point are considered "clutter" because they can appear at the same time as subsurface reflections.

Clutter cannot be removed from 2-D radargrams, but it can be mitigated. By comparing predicted clutter in a synthetic radargram, or "cluttergram," to SHARAD observations, one can determine which part of the signal is from the subsurface [*Holt et al*., 2006, 2008]. The cluttergram is calculated from a model of surface topography generated by Mars Orbiter Laser Altimeter (MOLA) data [*Smith et al*., 2001] and shows only the reflections that the radar will receive from the surface (Figure 6). Thus, reflections in the radargram that are not present in the cluttergram are considered subsurface reflections.

Orbital geometry with respect to surface topography exerts a strong influence on the amount of clutter received and the delay time of the first reflection. For our survey, favorable geometries are those where the

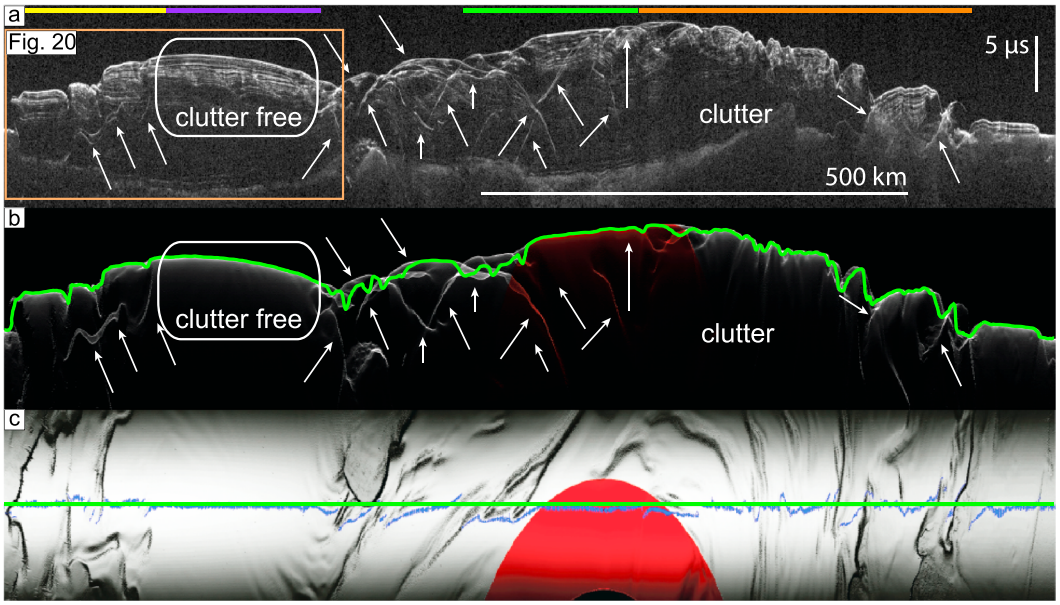

Figure 6. Comparison of radar data and clutter simulation. (a) Observation 725402 in one-way time. Arrows indicate clutter. Clutter-free section is discussed in Figure 20. (b) Simulated radargram matching Figure 6a. Clutter dominates the central portion of this image due to poor geometry of the orbital track relative to surface topography. Green line indicates NLPD surface topography along track. Red shading indicates region with only partial topographic data. (c) Shaded topography along the orbital track of radargram in Figure 6a. Brightness indicates relative strength of simulated echoes from the surface. Green line is ground track of spacecraft during this observation. Red area has partial topographic information. Blue shapes indicate the first reflection, sometimes offset from nadir due to surface geometry.

spacecraft ground track aligns nearly perpendicular to the strike of a trough. This results in first return surface reflections near the nadir point and less clutter. More oblique angles are less favorable, and radargrams from orbital track geometries aligning parallel to troughs are often unusable (Figure 6). We employ clutter mitigation techniques for all observations and present radargrams that are the most useful for interpretation.

3.3. Interpretation of 2-D Horizons and Correlating Reflectors

As of yet, individual reflectors cannot be directly correlated to specific visible layers [*Milkovich et al*., 2009], but due to correlative spacing and geometry, they can be used as a proxy for visible layering [*Christian et al*., 2013]. SHARAD reflectors are therefore assumed to be profiles of paleosurfaces of the former NPLD.

After mitigating clutter, reflectors are "picked" for time delay (t) and location (x, y). Picks are interpretations that correspond to a single reflector, or radar horizon. To track these reflectors, we employ a method similar to that performed by *Putzig et al*. [2009], using Schlumberger's seismic interpretation software package GeoFrame (Figure 7).

Due to the range resolution and sampling of SHARAD radargrams, a reflector may be spread over several pixels. To determine with greatest precision the location of that reflector, GeoFrame finds the highest-power pixel within 50 ns of the human-chosen picks. This "autopick" tool allows for faster and more accurate interpretations. Even with autopick, there is still subjectivity of interpretation because reflectors are often discontinuous at one or more points across the NPLD. A human interpreter must bridge the gap to create a complete horizon. To reduce uncertainty, we analyze multiple, crossing radargrams, allowing us to confidently correlate a reflector in one radargram to the same reflector in another, even if separated by a large discontinuity or by hundreds of kilometers (Figure 7). In many cases gaps can be circumvented entirely.

Few reflectors extend to the NPLD margin. Many disappear due to erosion or pinch out (Figure 2, dashes), and only the current surface and the lowest boundary, between the NPLD and the basal unit, are continuous across the entire cap. Therefore, it is impossible to map every reflector entirely without extrapolation. Because

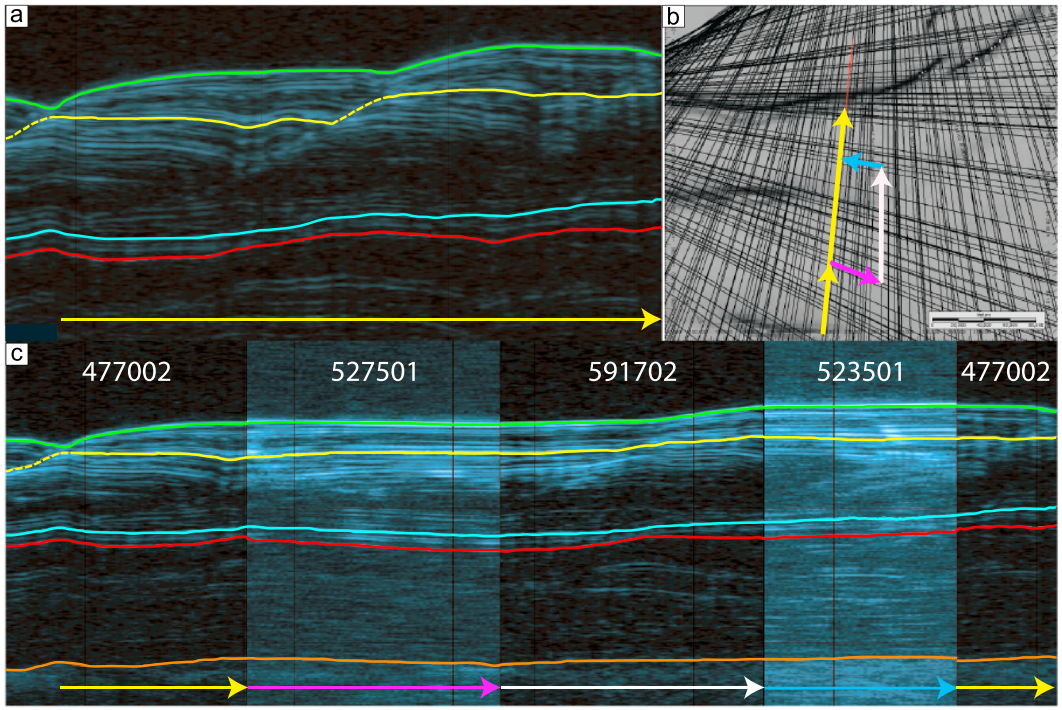

Figure 7. Technique for mapping around discontinuities. (a) Section of observation 477002. Three reflectors are interpreted: R29, R25, and an internal reflector (yellow) that crosses a TMP discontinuity (dashed). (b) Map view of observations in Figure 7c. Arrows indicate detour around TMP to avoid the discontinuity. (c) Connected observations 477002; 527501; 591702; and 523501. The yellow line is no longer discontinuous.

there is no other technique for estimating the surface represented by a single reflector that disappears in places, we extrapolate as sparingly as possible. Reflectors above and below the missing reflector provide geological constraints for estimating extrapolated surfaces.

Finally, we map the TMPs in order to study their variability in slope, vertical extent, etc. TMPs are identified by discontinuous reflectors, making them generally more difficult to trace. However, when observing geometries are favorable, TMPs are straightforward to detect. Once mapped, TMP properties can be analyzed for variability.

3.4. Geospatially Rectifying and Creating Surfaces

Once interpretation is complete, calculating the location of an individual reflector is critical for obtaining accurate *x* and *y* coordinates. Frequently, the reflection that reaches SHARAD first is not from directly below the spacecraft. This is especially true in regions with significant surface slopes. Using in-house software, we create facets of topography based on MOLA elevation [*Smith et al.*, 2001] for determining the closest point with appropriate aspect to the spacecraft. If a simulated signal is the first to reflect back to the receiving antenna, we call it a "first return," and the *x* and *y* coordinates are then moved to this facet (Figure 6c). The benefit of this technique is that the geometry determined by radar more closely reproduces that of the actual layers [*Christian et al.*, 2013].

The physical location of reflectors is critical to our analysis, and our picks must be converted from the time-based radargrams to depth. The *t* coordinate recorded by SHARAD is converted into *z* by employing equation (1).

$$d = \frac{c}{\sqrt{\varepsilon_r}} \times \frac{t}{2} \tag{1}$$

where *d* is depth, *c* is the speed of light, *t* is the two-way time as recorded by SHARAD, and ε_r is the real part of the permittivity or dielectric constant of the medium. For the subsurface position of the signal path, we employ an ε_r of 3.15 calculated for the bulk NPLD [*Grima et al.*, 2009].

Once the coordinates of each pick are properly rectified they are converted to a latitude, longitude, and radius point. These coordinates are imported into a geographic information system program such as Environmental Systems Research Institute's ArcMap for gridding. We interpolate each point into a raster grid using the natural neighbor algorithm in ArcMap. With this raster it is possible to study many properties of the surface, including topography, slope, aspect, and vertical separation from another surface.

To better convey reflector geometries in this paper, we primarily display depth-corrected radargrams. Depth correcting displays a more accurate reflector geometry, but it is also based on the assumptions described above. To reduce the uncertainty associated with those assumptions, our interpretations, as described in section 3.3, are done within the less processed time domain images. We then display the interpretations in depth.

4. Radar Observations

4.1. Regional Variability

Previous NPLD trough studies using SHARAD have focused primarily north of Chasma Boreale and near the margin at 90°E [*Smith and Holt*, 2010], but troughs elsewhere exhibit many of the same qualities. In order to understand troughs and ice accumulation around the cap, we extend those surveys to include the majority of the NPLD and offer a more holistic characterization of trough structure and variability. We divide the NPLD into eight unique regions based on a combination of surface and subsurface morphology, the latter taken from SHARAD observations (Figure 1). We discuss each in the following sections. The region within 3° of the pole lacks data coverage due to the MRO orbital inclination (Region 0, Figure 1).

4.1.1. Troughs in Region 1

Region 1 (Figure 1) exhibits archetypal trough migration as described by *Howard et al*. [1982] and *Smith et al*. [2013]. A wealth of good radar observations and straightforward stratigraphy makes Region 1 ideal to begin our survey, so we use these troughs as a standard example for comparison throughout this paper.

To demonstrate trough migration in three dimensions, we tracked five reflectors for their intersections with the TMP within many radargrams. The coordinates of each reflector's intersection with a TMP were recorded and converted to positions based on the techniques described in section 3. We chose progressively higher stratigraphic reflectors for sequencing the location of each intersection, including bright reflector R25 (light blue line in all other radar figures), the surface, and three others (Figures 8b and 8c). For a reference to reflector names and color codes, see Appendix A.

Projecting the points in map view demonstrates the troughs position and orientation. In this way we reconstruct each trough's relative (horizontal) motion through time (Figure 8a). The troughs generally migrated poleward, but migration is faster in some locations than others. Specifically, Trough 2, between time steps 2 and 3, migrated faster in the center than elsewhere. Between time steps 3 and 4, Trough 1 moved very little on the western end but migrated significantly in the east. An additional extension of Trough 2 appears between time steps 4 and 5, indicative of horizontal trough growth.

Smith and Holt [2010] observed that TMPs of troughs in Region 1 reached depths $>$700 m, intersecting R25. R25 is often discontinuous when it intersects TMPs, revealing that the troughs already existed at that stratigraphic level. Below R25, another bright reflector, R29 (shown as red in all figures containing radargrams), is more extensive and continuous than R25, i.e., R29 intersects TMPs less often than R25 (Figure 9). In our more extensive survey, we find values of accumulation and migration that are 50% greater than previous estimates. One trough in Figure 9b has migrated ~90 km during ~1100 m of accumulation. However, the migration to accumulation ratio is similar.

Even though troughs in Region 1 exhibit migration as described by *Howard et al*. [1982], geographic variability is detected. Near the center of Region 1, the high side of some troughs were only thinned and not fully eroded, resulting in reflectors that are not discontinuous. Hence, the TMP is not a true bounding surface, yet successive stratigraphic inflections indicate the migration path of those troughs (Figures 2b, rightmost trough, and 8c, Tr 1). The TMP of these troughs begin above R25, evidence for relatively late lateral trough growth (see Figure 8a time step 4).

Most Region 1 troughs exhibit asymmetric accumulation similar to that depicted in Figures 4 and 5a. An anomalous migration can be found on the low side of some Region 1 TMPs. *Smith and Holt* [2010]

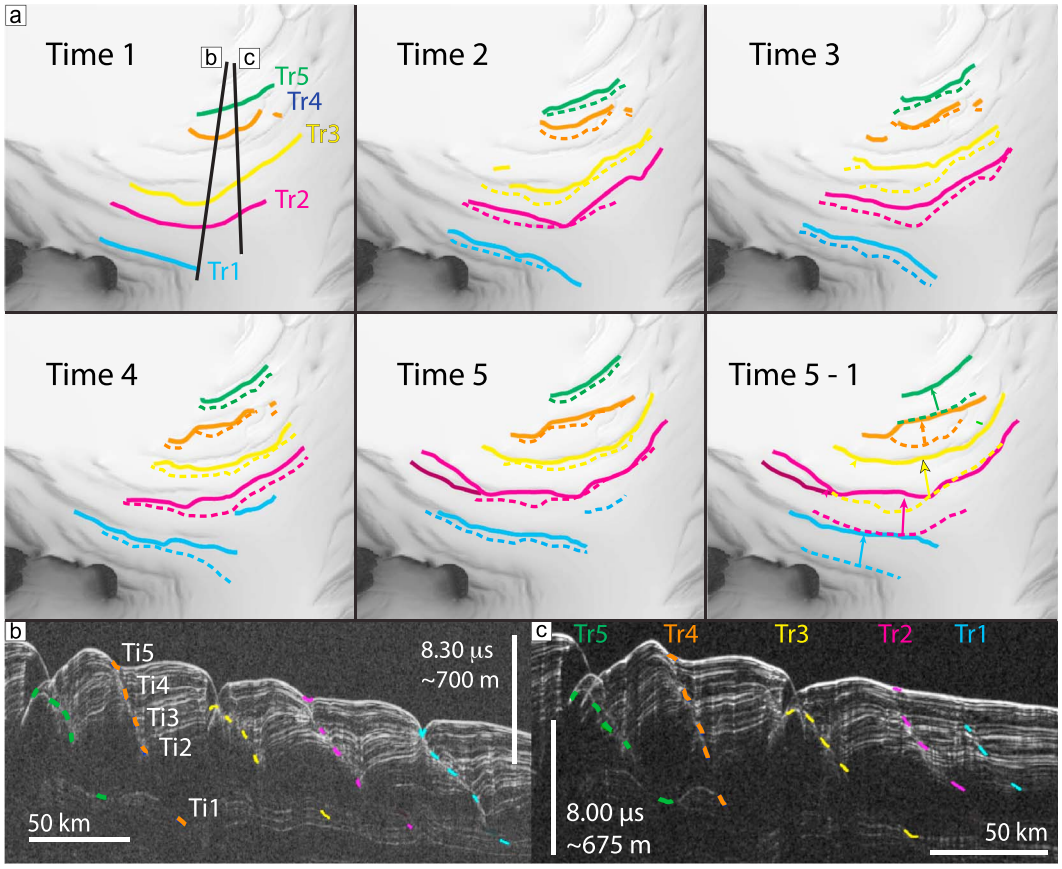

Figure 8. Map view of trough migration. (a) Locations of five Region 1 troughs at five time steps. Colors indicate individual troughs. To show the difference between time steps, solid lines match the location of trough at the time step listed, and dashed lines are the trough's position at the previous time step. (b) Portion of SHARAD observation 933202 showing reflectors that intersect with the TMP at times corresponding to Ti1–Ti5. (c) Portion of observation 706402 showing each trough in respective color. Comparing Figures 8b and 8c shows that the eastern extent of Tr1 and Tr2 did not form at the same time as the western end. Tr1 has no surface expression. The lowest point for Tr3–Tr5 corresponds to where the TMP meets R25.

characterized this type of anomaly as "V shapes," exhibited by several 100 s of meters of reflectors that dipped downward followed by concave up reflections (Figure 2c from that paper). At the TMP we detect former ledges or buried promontories in this migration (Figure 9b) similar to the cartoon of migration in Figure 5d.

4.1.2. Troughs in Region 2

Region 2 troughs share many attributes with those in Region 1. On the surface they display similar layered and banded terrain, and their wavelengths are approximately the same. However, they are more complicated, generally having deeper, W-shaped cross sections due to central promontories. We call these compound troughs (e.g., "CT" in Figures 10b and 11b). In addition to surface promontories, SHARAD detects two promontories buried by ~250 m of material during migration (Figure 11b). Both promontories exhibit horizontal reflectors (yellow), contrasting the sloping layers deposited above, indicating the depositional geometry prior to the erosion that created the promontories.

Figure 10b spans Region 1 and Region 2. At the highest latitudes (Region 1) classical migration is displayed. Farther south, near Chasma Boreale (Region 2), the troughs are deeper—as much as 1 km. TMPs are visible and indicate that the two lowest-latitude troughs in Figure 10b have migrated 16 and 24 km, respectively. Here reflector separation on the high side of each trough decreases, indicating thinning, but the low side does not show strong thickening, in contrast to Region 1 troughs. We also detect a familiar V-shape geometry at the same two lowermost troughs in Figure 10b (magenta reflectors).

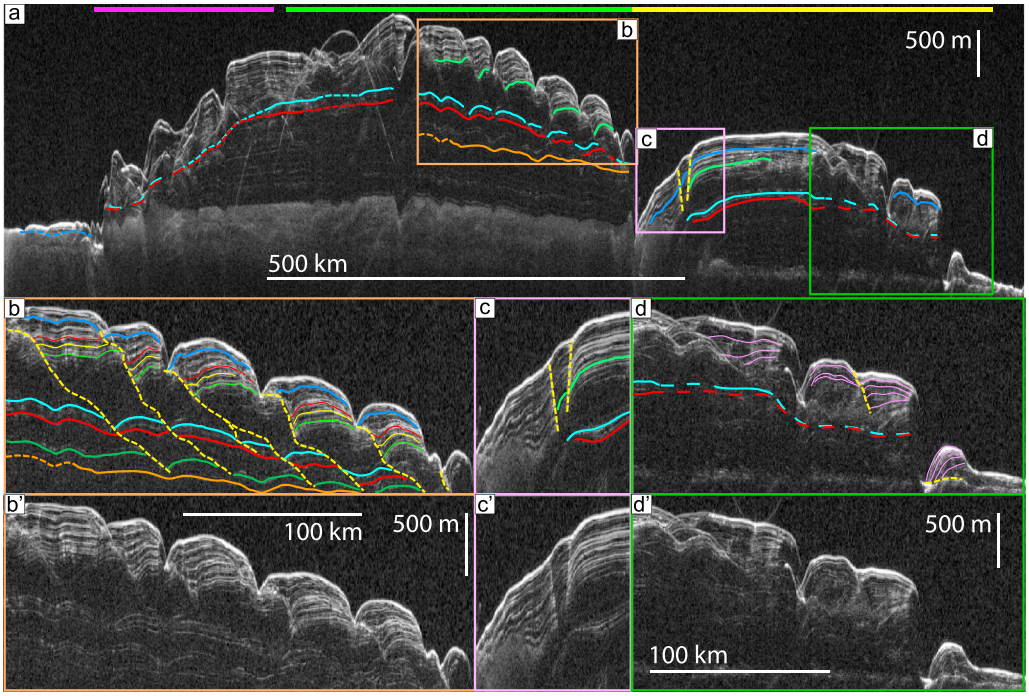

Figure 9. Observation in Regions 4, 1, and 7. (a) SHARAD observation 1252401 with interpretations: R29, R25, and R17. Region 4 (left) has significant clutter due to poor observation geometry. (b) Section of Figure 9a in Region 1. Some troughs display V-shaped geometries (Figure 5d). Reflectors below TIS-1 are offset (dark green), signifying that the oldest troughs on the NPLD migrated as many as 90 km since initiation, some 1100 m beneath the current surface. (c) Observation of Region 7b minor troughs. One migrated downstream, contrary to most TMP. (d) Observation of Region 7a. Layers exhibit thinning on the high side and thickening on the low side for normal trough, but the marginal trough with a bedrock base exhibits thinning on the low side (magenta) and migrated horizontally over the bedrock.

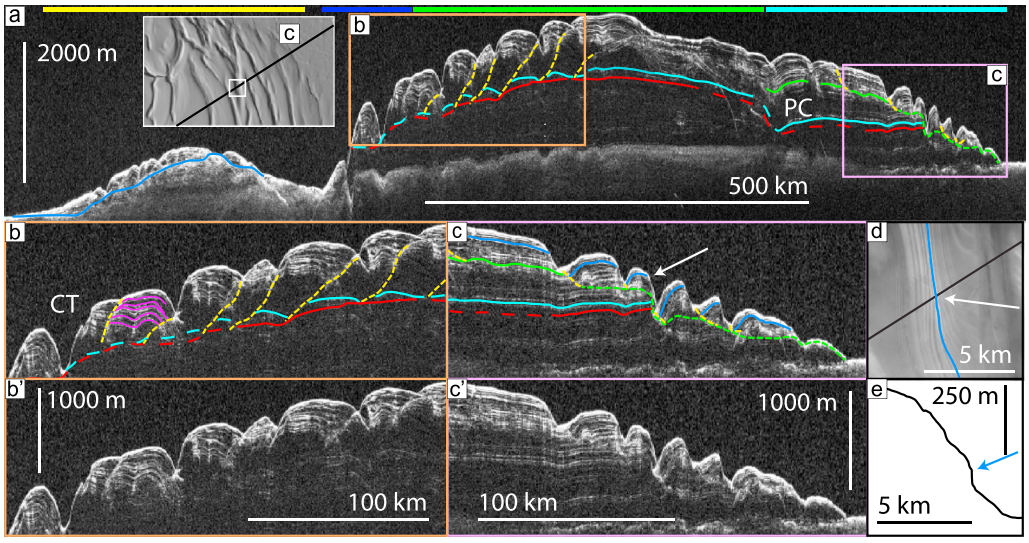

Figure 10. Observation 855602. (a) Regions 7, 2, 1, and 5. Inset is hillshade section of Region 5 with footprint of Figure 10d. Black line indicates ground track of Figure 10c. A large paleochasma (PC) is easily observed in this image. Regional slopes point toward the pole, precluding katabatic winds and jumps. (b) Regions 1 and 2. Troughs have easily identified TMP. One compound, W-shaped trough (CT) is exhibited in Region 2. (c) Region 5. TIS-2 (green), associated with R17 is stratigraphically higher than TIS-1. R25 and R29 are truncated at TIS-2 erosion. White arrow identifies unconformity in Figure 10d. (d) Portion of CTX image P20_008991_2644_XI_84N267W. Black line is ground track of 855602. White arrow identifies an unconformity mapped by *Tanaka and Fortezzo* [2012] that may appear in Figure 10c. (e) Topographic profile of Figure 10d with arrow indicating elevation of unconformity.

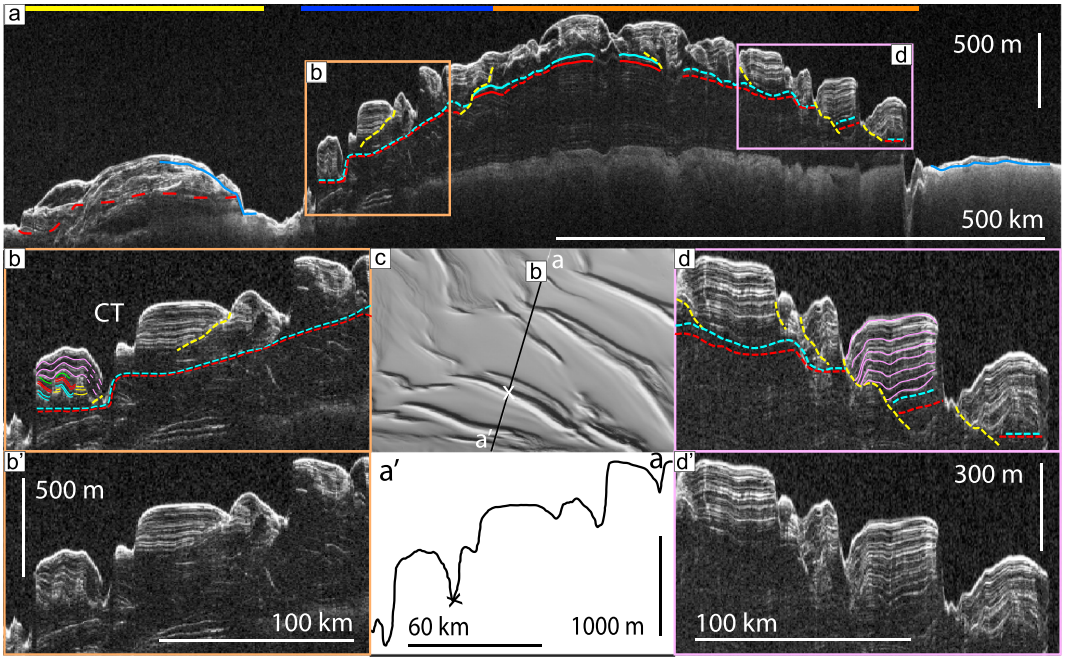

Figure 11. Observation 2265701. (a) Interpreted Regions 7, 2, and 3. (b) Troughs in Region 2 exhibit TMP and minor thickness variations. They also exhibit a central promontory on the surface (CT). Migration over formerly exposed promontories is detected (magenta). (c) Hillshade of Region 2 with SHARAD ground track and topographic profile. The lowest point is marked by an X. (d) Region 3: TMPs and thickness variations are visible. V-shaped layers are present at one trough.

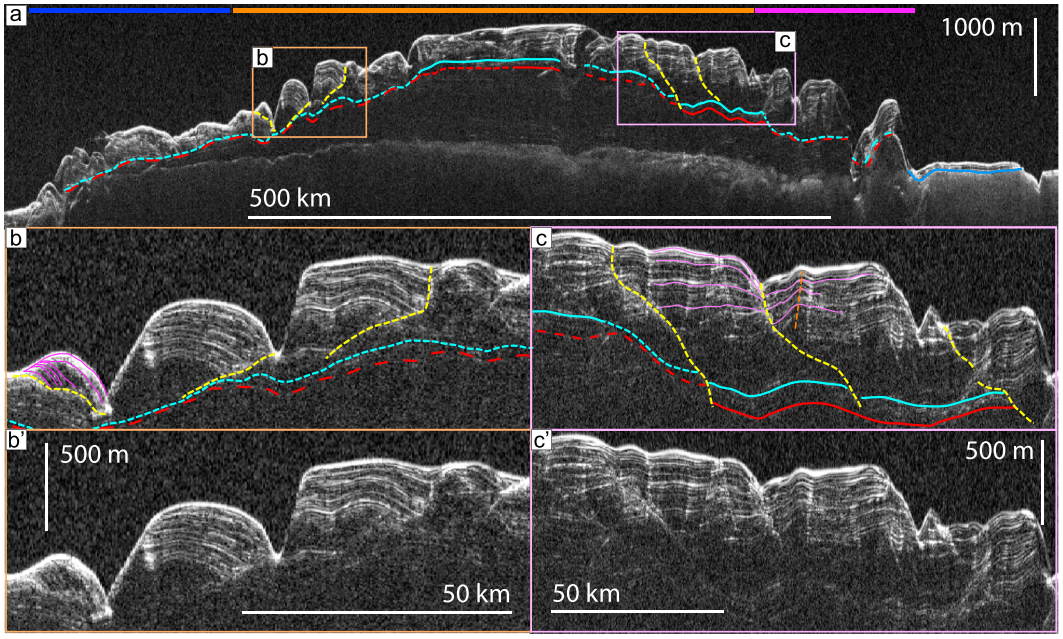

Figure 12. Observation 2189301. (a) Interpreted Regions 2–4. (b) Three TMPs from Region 3. The southernmost trough migrated downward, matching predictions of marginal troughs [*Howard et al.*, 1982]. (c) Trough near 205° migrated northward, while nearby undulation migrated southward. In each region the TMPs approach R29.

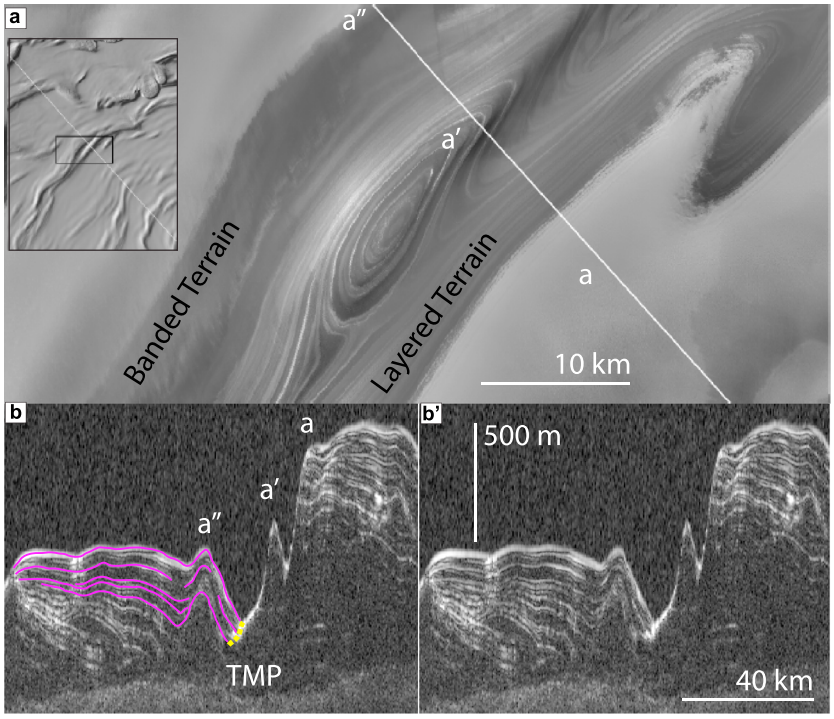

Figure 13. Observations of trough with central promontory and interpacket material. (a) Portion of CTX image B01_010014_2644_XN_84N107W. Layers can be traced around the central promontory. Banded terrain near a″ demonstrates deposition associated with trough migration. Line is ground track of Figure 13b. Inset shows location on NPLD. (b) Portion of observation 556602. Except for W shape, trough exhibits familiar features: TMP and asymmetric accumulation. Layers of recent accumulation onlap and drape a second promontory at a″. Low reflectivity interpacket material described by *Putzig et al*. [2009] reaches the surface below a′.

Continuing west, Figure 11b shows deep compound troughs and evidence of migration. Near the mouth of Chasma Boreale, at 315°E, one well-delineated TMP indicates ~30 km of migration. Layers near the TMP thin as they approach from the high side but have reduced low side thickness variation.

4.1.3. Troughs in Region 3

Region 3 offers greater diversity from the troughs of Region 1, with more variable wavelengths and trough depths. Troughs are deepest nearest the NPLD margin, sometimes reaching depths of ~1 km. Topographic undulations dominate the intertrough plateaus of this region.

At 289°E, near the border with Region 2, three troughs display well-defined migration paths that begin near R25 (Figure 12b). These troughs have migrated northward 17, 17, and 19 km during ~500 m of accumulation. The lowest latitude TMP in Figure 12b shows an anomalous downward inclination. Each of these troughs is associated with reduced thickness variations between reflectors compared to Region 1 (cf. Figures 5a and 5b). At even lower latitudes, the troughs have extremely low relief (Figure 12a).

At 227°E, 86.5°N, another trough displays a well-defined TMP, sloping layers, and thickness variations (Figure 3c). The TMP is particularly easy to identify here because the low-side layers are adjacent to a section with few reflections. High-side layers only thin in the top ~110 m (above the dark blue reflector). On the low side, the TMP shallows in slope at the same stratigraphic level. Below 110 m layers vary too little to detect, similar to Figure 5b. Figures 11d and 12c exhibit several TMPs. Below the uppermost bright reflectors, R25 and R29 are discontinuous across the TMP, revealing that the trough existed prior to R29. Magenta colors show subdued V-shaped reflectors that characterize the trough in Figure 11d. During >250 m of accumulation, this trough migrated ~30 km laterally.

A trough that has been the subject of some debate [*Rodriguez and Tanaka*, 2011] resides at 252°E and 84.5°N (Figure 13a). The central promontory, around which layers can easily be traced, contributes to the confusion. This trough and others have been interpreted to form during in situ erosion, without migration

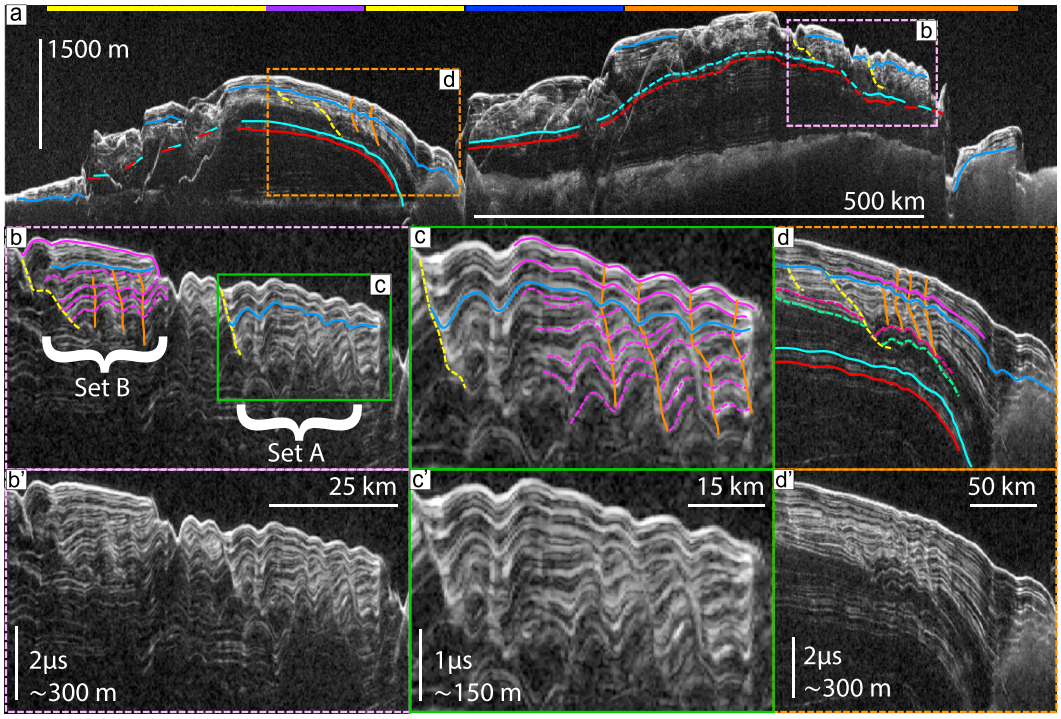

Figure 14. Observation 2007101 in Regions 7, 6, 2, and 3. (a) Observation of R29, R25, and some TMPs. Region 2 is obscured by clutter. (b) Two sets of undulations are seen in Region 3 down to ~2 μs (~300 m; Sets A and B). Both sets migrated northward ~6 km until 0.6 μs delay time (~90 m) beneath the current surface where Set A changed migration direction and Set B was buried. (c). Erosion exposed layers on the surface prior to reversal (blue line). (d) Migration is observed for trough and undulations in Regions 6 and 7. Region 7 trough becomes buried, and undulations reverse migration ~100 m beneath surface. R25 and R29 intersect the bedrock at a steep angle. Figures 14b–14d are displayed in time to demonstrate the undulation migration without distortion from depth correcting.

[*Rodriguez and Tanaka*, 2011]; however, a closer look reveals that all of the standard migration characteristics are visible. Layered terrain is expressed down to the lowest portion of this trough, between a′ and a″ and is ~400 m lower than the central promontory at a′. On the low side, banded terrain is observed at a″. SHARAD results provide additional information. Thinning high-side reflectors contrast thickened, pole-tilting reflectors on the low side (Figure 13b). A short but otherwise clear TMP is observed. There is also a previously undiscussed promontory, buried by ~150 m of material during migration. This promontory has approximately the same dimensions as the promontory at a′ but has a reduced surface expression due to burial. Finally, the surface peak above the buried promontory is 1.5 km north of the buried peak, further indicating migration.

The surface of Region 3 is rich in topographic undulations. *Smith et al*. [2013] suggested that undulations were related to trough formation, and *Herny et al*. [2014] provided an initial stratigraphic analysis but did not demonstrate migration. Both studies concluded that undulations form during the same wind regime as troughs but are fundamentally different. We find stratigraphic records in SHARAD revealing migration associated with undulations.

Figure 14b shows two sets of undulations that formed at approximately the same time as nearby troughs, reaching 500 m beneath the current surface to approximately R25. Between 500 and 90 m beneath the surface, both sets migrated northward. Then at ~90 m, both sets experienced minor erosion. Afterward, Set A switched migration direction (Figure 14c), while Set B became buried, leaving no surface expression (Figure 14b). Independent of migration direction, the wavelength of both sets remains approximately constant at ~6 km, throughout accumulation.

4.1.4. Troughs in Region 4

Observations of troughs in Region 4 (Figure 1) are more difficult to make with SHARAD than in other regions due to poor observation geometry, which results in significant clutter. Furthermore, this region has

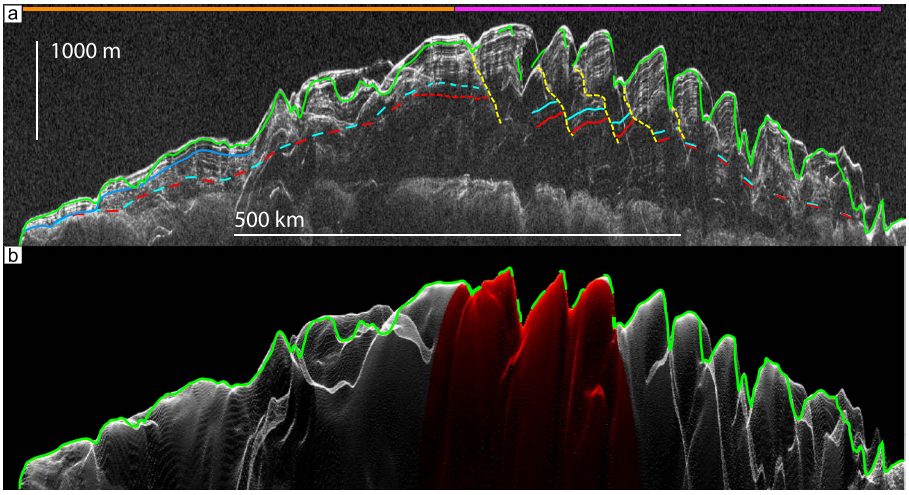

Figure 15. Radar image and cluttergram for observation 1087102 crossing Regions 3 and 4. (a) Poor observation geometry makes interpretations difficult; however, some TMPs intersect R29 and R25, demonstrating an age of onset that predates most NPLD troughs. (b) Cluttergram for observation 1087102 showing significant clutter. Central portion, corresponding to where topography data are incomplete, is colored red. MOLA-derived topography is shown as green line.

undergone large-scale erosion and deposition (discussed below), making subsurface structure difficult to interpret.

Figure 15 details the amount of clutter visible in a radargram with moderately favorable geometry. The highest-latitude troughs display discontinuous reflectors R25 and R29, indicating that trough formation preceded deposition of R29. Lower latitude troughs are impossible to interpret with confidence. R29 and R25 are incompletely detected due to significant erosion that likely removed them.

4.1.5. Troughs in Region 5

Region 5 is unique when compared to other regions. First, reflectors R29 and R25 are traced throughout Region 5, but neither reflector exhibits discontinuities associated with TMPs, implying that the troughs initiated later than in other regions (Figures 10c, 16, 17b, and 18) [*Smith and Holt*, 2010]. R25 is continuous and convex up, conformable with and filling in the paleochasma described by *Holt et al*. [2010]. Above R25, as many as 600 m filled the paleochasma before the first TMP is detected.

The second distinguishing feature of Region 5 is that the troughs initiated after widespread erosion. Stratigraphically above R25 and subsequent deposition, an angular unconformity cuts layers near trough initiation (Figures 10, 16, 17, and 18, green). Layers beneath the unconformity are truncated without thinning, whereas layers immediately above the unconformity onlap at angles. Trough stratigraphy arises in Region 5 immediately above the unconformity.

The erosion associated with trough initiation is extensive, spanning the entire longitudinal breadth of Region 5, more than 650 km, from 18° to 104°E (Figure 1b), corresponding to the eastern portion of Gemini Scopuli

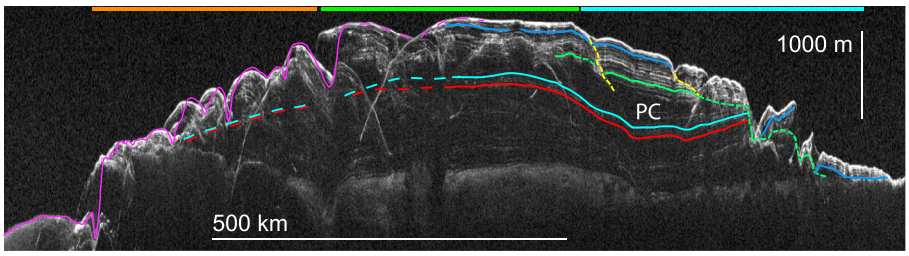

Figure 16. Observation 1044302 of Regions 2, 1, and 5. Left of image corresponds to Regions 1 and 2, where poor observation geometry results in clutter. In Region 5 there is clear evidence of erosion (R17, TIS-2). Reflectors R25 and R29 reach the surface at a scarp. MOLA topographic profile is shown in magenta to demonstrate influence of clutter.

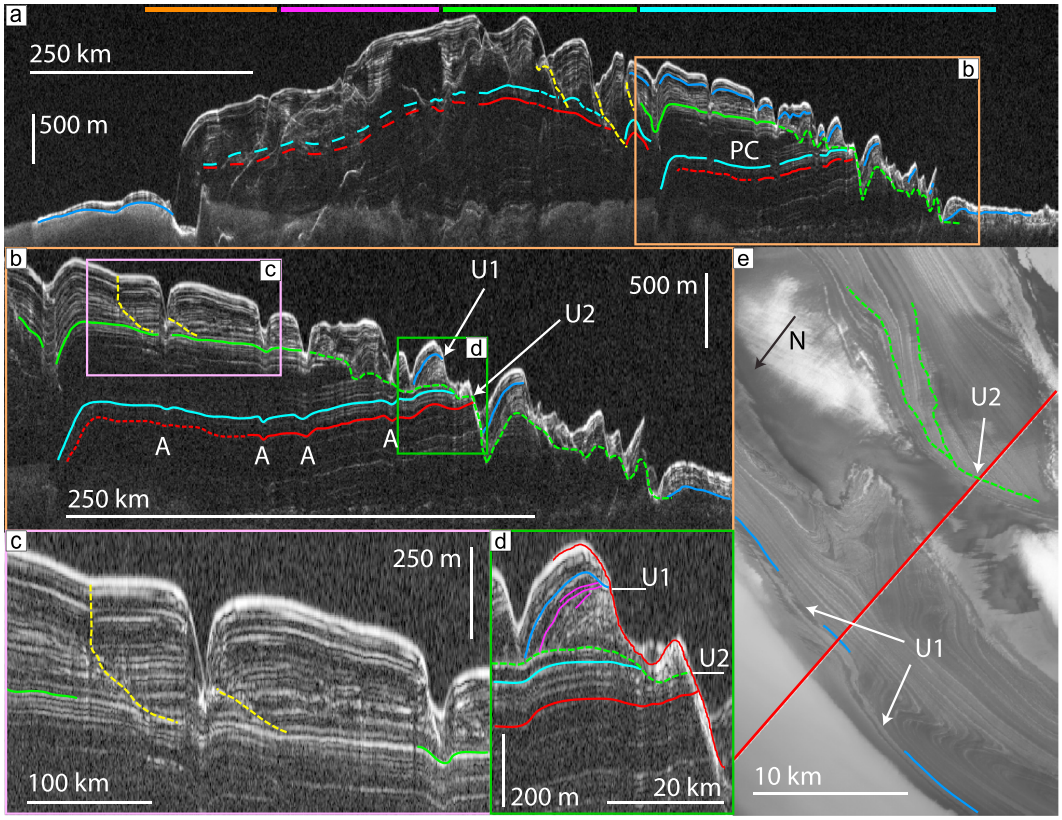

Figure 17. Observations of troughs. (a) SHARAD observation 761602 in Regions 3, 4, 1, and 5. Center left: Region 4 is obscured by clutter. Center: Region 1 exhibits TMPs. A large break in R25 and R29 shows the discontinuity during deposition caused by the paleochasma (PC). Right: Massive erosion (dashed green line) predated trough formation in Region 5 near R17. (b) Region 5 observation showing more detail from Figure 17a. Radar processing artifacts (A) show up beneath the troughs and do not represent the true geometry of the reflectors. All Region 5 troughs initiated immediately after the erosion that coincides with bright reflector R17. (c) TMP slope increases significantly from 0.93° to 12° as in Figure 5c. (d) Two contacts (U1 and U2) are detected that correspond to mapped unconformities in Figure 17e. Red line is MOLA topographic profile at nadir. (e) CTX image P01_001529_2622_XN_82N288W exposing two unconformities [*Tanaka and Fortezzo*, 2012]. Arrows correspond to Figure 17d. Exposed layers to the right of U2 are NPLD material that predates TIS-1.

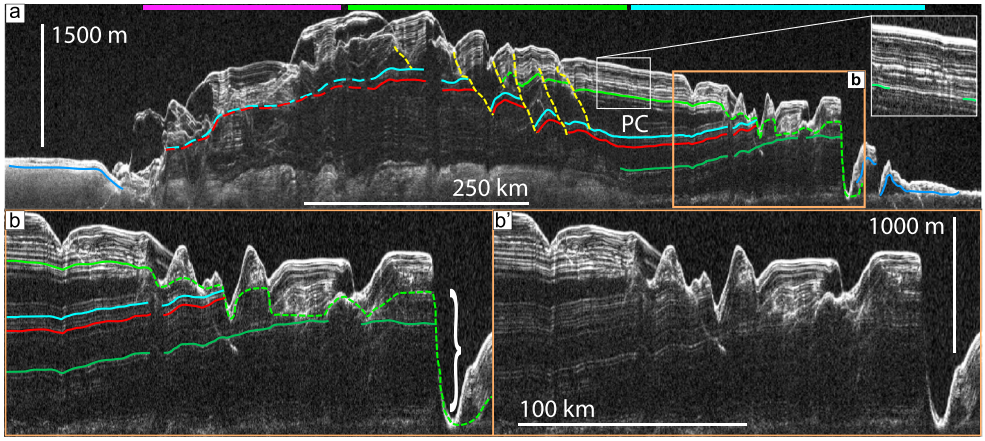

Figure 18. Observation 1982701 in Regions 4, 1, and 5. Region 4 has abundant clutter. TMPs are easily identified in Region 1. Observation crosses the Region 5 paleochasma (PC) that predated troughs. Inset: relative brightness of R17 compared to other reflectors. One brighter reflector is found above. (b) Erosional surface that predated Generation 2 troughs is highlighted. Significant amounts of pre-TIS-1 material reach the surface at a scarp (white bracket). R25 and R19 are also exposed at a scarp.

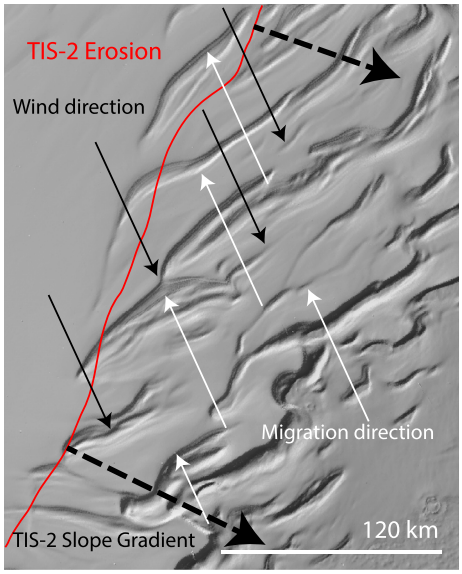

Figure 19. Region 5: wind directions [from *Howard*, 2000] align antiparallel to migration direction. Strike of TIS-2 erosion (red line) is not orthogonal to winds, demonstrating that troughs migrate upwind, not necessarily upslope.

[*Tanaka and Fortezzo*, 2012]. Tracking this erosion eastward from ~100°E is difficult due to clutter and complex depositional history associated with Region 4. Westward of ~20°E, at the Region 7a boarder, the scarp angle becomes too low to differentiate from horizontal layering (Figure 2). In latitude the unconformity extends from ~84°N to the NPLD margin. The northernmost extent of erosion parallels the highest-latitude troughs throughout Region 5, giving it a somewhat linear appearance (Figures 1b and 19). The troughs have since migrated northward to their current location.

Many unconformities have previously been identified within Gemini Scopuli [*Tanaka and Fortezzo*, 2012], providing useful stratigraphic context for SHARAD mapping. It is notoriously difficult to colocate optical imagery and SHARAD due to SHARAD's lower horizontal resolution. However, exposures on the NPLD are sometimes large enough that an isolated, individual contact can be found in both SHARAD and optical instruments. We sought these locations and exposures of older, pretrough NPLD material.

On the high side of a trough at 70.2°E, 82.3°N, an unmantled exposure of layered terrain exists (Figure 17e). It is ~300 m tall and approximately 17 × 9 km in area, large enough that a radargram footprint can confidently be placed within the boundary. Optical imagery reveals an unconformity (U2) on the trough high side [*Tanaka and Fortezzo*, 2012], and mantling is observed north of the unconformity.

At the same location, SHARAD reflectors R29, R25, and others approach the surface, in agreement with layers exposed in imagery (Figure 17d). R25 is truncated at an unconformity and mantled at an elevation that corresponds closely to U2. Because of these agreements, we interpret R29 as reaching the surface somewhere between U2 and the bottom of the trough. Layers below R19 are much older than those above U2. They appear to be of typical albedo and thickness for the NPLD.

Higher on the trough slope, there is a change in layer properties near another unconformity (U1; Figure 17e). Stratigraphically below the contact, layers have no evidence for wind streaking, but above the contact, layers appear to be scoured by winds. SHARAD detects an unconformity at approximately the same elevation (Figure 17d). Because an isolated unconformity is detected both in radar and imagery, we interpret them to be the same.

4.1.6. Troughs in Region 6

The Region 6 surface is one of the smoothest places on the NPLD, an unlikely place to find troughs. However, SHARAD observations with favorable geometries find more detail in the subsurface. Here we present the first clear evidence of buried troughs in the NPLD.

Figure 20 displays radar reflectors indicating familiar characteristics: TMPs and asymmetric accumulation. Four migration paths are evident during ~600 m of deposition, showing two distinct troughs with wavelengths of ~50 km and indication of a third. The highest trough (toward the center of Gemina Lingula) migrated ~40 km, and the next two migrated ~65 and 60 km, respectively. These troughs have stratigraphy comparable to troughs in Region 1, including onset near R29. Figure 14d also shows a buried trough in Region 6.

These troughs differ from troughs in all other regions. First, at ~110 m below the surface the troughs transition from being easily detected to nonexistent, as their TMPs disappear and are replaced by parallel, subhorizontal reflectors. Second, the TMPs in Figure 20 indicate that the troughs migrated southward prior to burial rather than northward.

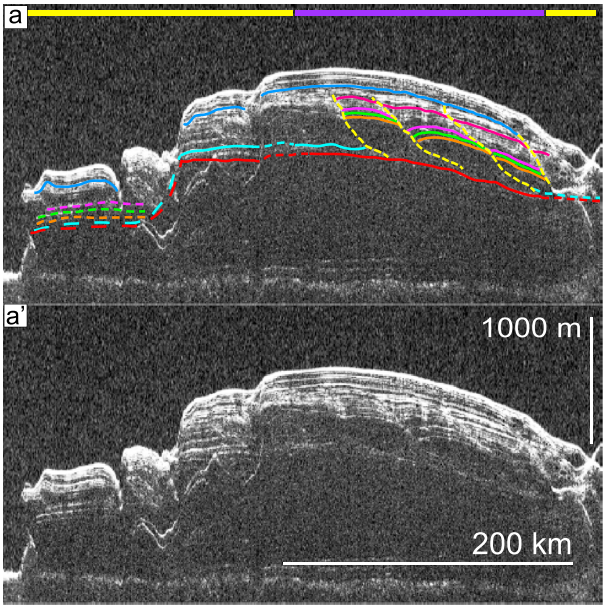

Figure 20. (a) Observation of buried troughs in Region 6 (from Figure 6). TMPs and layer thickness variations reveal that several troughs once migrated equatorward, opposite in sense to almost all other troughs on the NPLD. The ~50 km wavelength troughs are now buried beneath ~100 m of material. Buried troughs are incompatible with a flowing-ice scenario for the NLPD (see Figure 23). (a′) Uninterpreted observation with scale bars.

4.1.7. Troughs in Region 7

Region 7 shares characteristics with other regions, including extensive undulations, as in Region 3; marginal troughs and scarps similar to Region 5; and unfortunately, Region 7 shares extensive erosion with Region 4, which, combined with unfavorable observing geometry, makes it difficult to interpret. Furthermore, troughs in Region 7 are more sparse than in other regions, resulting in no more than three consecutive troughs within a single radargram (Figure 9).

We subdivide Region 7 into two portions. Region 7a encompasses the troughs on the Gemina Lingula southern margin associated with Gemini Scopuli. Many of these troughs are deep enough to reach bedrock beneath the NPLD (Figure 9). Region 7b borders Chasma Boreale to the south. Troughs here are less mature than in other regions but still exhibit characteristics of migration (Figure 9c). Topographic undulations exist in both subregions, but few have sufficiently good geometries to be detected by SHARAD [*Herny et al*., 2014] (Figures 14d and 2).

In Region 7a, poleward tilting deposits are exhibited on the low side of each marginal, bedrock-reaching trough (Figure 9d). Reflector separation thins on the low side, contrary to the standard trough. Nevertheless, reflectors on the high side display conventional thinning, possibly indicative of processes unique to marginal troughs [*Howard et al*., 1982; *Pathare and Paige*, 2005]. Having a bedrock base adds another complication to our interpretations. TMPs usually indicate accumulation during migration, but the ablation portion of these troughs is at the erosionally resistant bed, so migration is forced to be horizontal. This is also true for some Region 5 marginal troughs (Figures 17b and 18).

Minor troughs are observed in Region 7b, on the northern side of Gemina Lingula. A minor trough has a small cross section and distinct TMP (Figure 9c). These are distinguished from undulations primarily because they are isolated, and reflectors are more discontinuous. Minor troughs throughout Region 7b have TMPs down to a level higher than R25. In Figure 9c, the two minor troughs migrated nontraditionally: one has a rare, vertical migration and the other has always been migrating down slope.

4.2. Trough Initiation Surfaces

To better understand the morphology of the NPLD around the time of trough initiation, we mapped an approximate surface around which the majority of troughs initiated. In Region 1, the timing of initiation was variable, from prior to R29 (Figure 9b) to post R25 (Figure 8c), so no one stratigraphic level can be considered a true formation surface. However, R25 is close to the time at which most NPLD troughs formed, and we refer to R25 as trough initiation surface one (TIS-1).

Across much of the NPLD, TIS-1 is either continuous or broken by only small segments, making layer analysis straightforward (Figure 2). However, in some regions, specifically at the boundary of Regions 1 and 5 (Figures 10a and 17a), large offsets and weak radar reflections make connecting R25 difficult. To compensate, we sought radargrams that connected R25 across this boundary (Figure 16) and supplement that with intersecting radargrams to map around the discontinuity as shown in Figure 7.

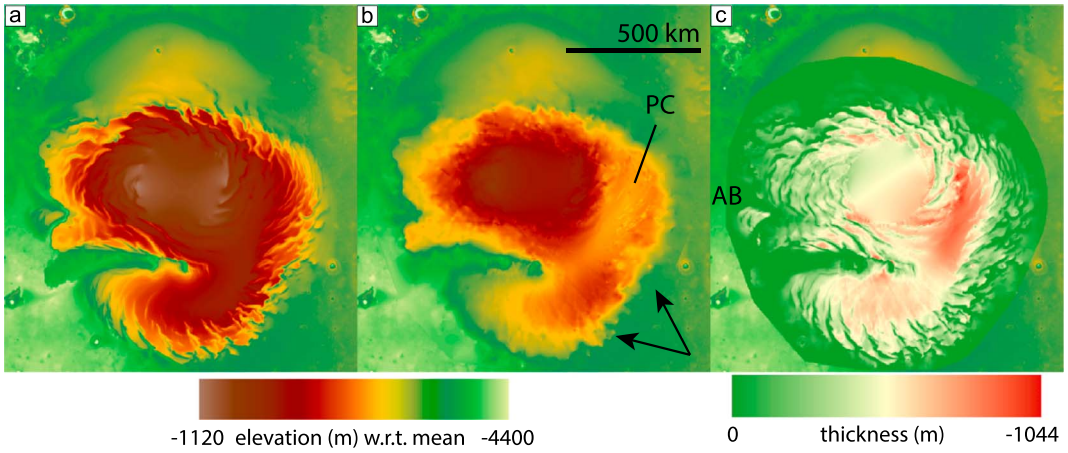

Figure 21. Topography and accumulation of NPLD. (a) Current topography from MOLA [*Smith et al.*, 2001]. (b) Topographic map created by interpolating R25 from ~400 observations per methods in section 3. Erosion near the margin in Region 5 (black arrows) and the paleochasma (PC) and are evident. Katabatic acceleration is hindered because of the poleward facing slopes on the southern portion of the paleochasma (as discussed in section 5.1). Color scale for Figures 21a and 21b was chosen to maximize detail. (c) Accumulation between TIS-1 and current MOLA surface. Accumulation was greatest near the paleochasma. Intertrough plateaus also accumulated significantly. Relatively little accumulation occurred over at the highest portion of the NPLD (current and former) or near trough bottoms. Abalos Mensa (AB) developed with uppermost NPLD material [*Brothers et al.*, 2013].

Since R25 extends to the NPLD margins in only a few locations, an incomplete survey results. In certain areas, specifically south of 86°N in Regions 3 and 4, R25 has likely been removed by erosion. Using methods described in section 3 for creating surfaces, including comparing reflectors in geologic context, we extrapolate R25 toward the margin (blue dashes in figures containing radargrams) to estimate the size and shape of the NPLD at the time of TIS-1 (Figure 21b).

Troughs that did not form around the time of TIS-1 formed stratigraphically higher in Regions 5 and 7a. Region 5 is easiest to interpret. These troughs initially formed on a surface described by widespread erosion that was contemporaneous with a reflector R17 (Figures 1b, 10, 16, 17, and 18). Immediately above the unconformity (trough initiation surface two (TIS-2)) every Region 5 trough initiated.

Determination of trough initiation in Region 7 is difficult because of poor observation geometries and lack of a distinct initiation surface. Trough initiation on the southern margin is either obfuscated by clutter or within a zone of low reflectivity. Minor troughs in Region 7b all initiated subsequent to R25 but prior to R17 (Figures 3a and 9c) and may be considered Generation 1 troughs.

With TIS-1 and TIS-2 well described, we learn that at least two major periods of trough formation occurred on the NPLD. First generation troughs arose as the NPLD accumulated material, while the second generation arose abruptly, following the removal of large quantities of material from the NPLD. Even though Generation 2 troughs followed an erosional event, they formed during a period of accumulation.

We measure the initiation slope in each region for later discussion. In Region 1, the average trough initiation slope for all observations is 0.19°. In Region 2, the slope varies by longitude (Figures 10b and 11b). We find an average of 0.27°. Region 3 troughs initiated near TIS-1 (Figures 12 and 14), which we use to find the average initiation slope of 0.27°. Region 4 troughs formed prior to the deposition of R29 (Figure 15), but the slope is difficult to measure confidently. We estimate from Figure 9 and find that the initiation slope rises ~1100 m over ~150 km, ~0.39°.

TIS-2 slope varies by location. Eastern and central portions were eroded more strongly than those of the far west, where either the unconformity becomes difficult to distinguish (Figures 2c, 14a, and 20) or very steep scarps show the removal of all ice back to the new margin (Figures 18 and 21b). The initiation slope varies longitudinally from 0.27° to 0.39°, averaging 0.32°. Some of that variation may be due to observation geometry not matching the true dip direction.

Table 1. List of Observations and Measurements From Each Region

Region	Observation	Initiation Slope (deg)	Average Slope (deg)	Standard Deviation (deg)	Nominal Wavelength (km)	Wavelength Error (km)
Region 1	2197801	0.20				
Region 1	1207501	0.22				
Region 1	1294501	0.22	0.19	0.033	47	5
Region 1	1247002	0.15				
Region 1	1247102	0.16				
Region 2	1844601	0.22				
Region 2	1280202	0.26				
Region 2	1837301	0.23	0.27	0.078	36.5	5
Region 2	1321501	0.41				
Region 2	1818202	0.25				
Region 3	1321501	0.27				
Region 3	2268301	0.25				
Region 3	2356401	0.26	0.27	0.026	37.15	10
Region 3	725402	0.31				
Region 4	1087102	0.19				
Region 4	1247102	0.43	0.32	0.122	35	5
Region 4	1252401	0.34				
Region 5	1280202	0.27				
Region 5	1837301	0.30	0.32	0.051	24.5	5
Region 5	761602	0.31				
Region 5	855602	0.39				
Region 6	725402	0.12				
Region 6	923202	0.14	0.13	0.014	50	5

Region 6 TMPs are traceable down to between R25 and R29 and initiated on a relatively low slope of 0.13° (Figure 20). As discussed in section 4.2, we are unable to estimate the initiation slope in Region 7. To compare all initiation slopes measured versus wavelength, see Table 1 and Figure 22.

4.3. Volume Estimates

By comparing the current MOLA measured surface to that of TIS-1 (Figure 21), several observations are readily apparent. Chasma Boreale existed as the troughs were forming, but it was much shallower than it is currently. The paleochasma first described by *Holt et al*. [2010] east of the saddle region had been partially filled in. The highest elevation on the NPLD (with mapping limited to latitudes south of 88°N) was not centered at the pole. Instead, it was nearest 270°E, continuing the trend from before the NPLD began depositing [*Putzig et al*., 2009].

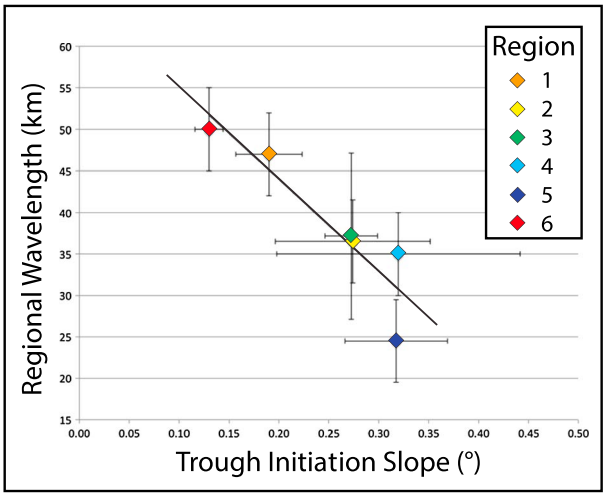

Figure 22. Plot of trough regional wavelength versus trough initiation slope. Troughs that form on lower regional slopes have longer wavelengths. Slope error bars are standard deviation of averaged values (Table 1). Wavelength error bars are set to 5 km except in Region 3, where they are set to 10 km due to large variability.

From this mapping, we estimate the volume of the NPLD near the deposition of TIS-1. Assuming a flat base of the "basal unit," or Rupes Tenuis, we find that ~7×10^{14} cubic meters of ice and dust had already been deposited.

We subtract the elevation of TIS-1 from the MOLA surface to determine

the pattern of accumulation and the volume of ice and dust that has accumulated since trough onset (Figure 21c). Approximately 3×10^{14} m^3 have been deposited in that time. This number is larger than the volume calculated by *Putzig et al.* [2009] (2.33×10^{14} m^3) even though it roughly corresponds to the same unit (G in that study). We attribute this difference to the mapping methods used (ours described in section 3 above) and find the volume from *Putzig et al.* [2009] to be an underestimate because their mapping crossed stratigraphic boundaries. Our value is approximately one third (1/3) of the total volume of the NPLD. Because of the aforementioned erosions and material lost in Regions 3–5 and 7, the volume accumulated since TIS-1 should be lower than the total volume deposited during that period.

The greatest accumulation has occurred at the boundary of Regions 1 and 5, above the buried chasma, totaling over 1000 m locally. Other locations that have accumulated significantly are between troughs (highest local points) and Gemina Lingula. Abalos Mensa developed in that time, agreeing with the conclusion of *Brothers et al.* [2013].

The locations that have received the least amount of accumulation are at the bottoms of present-day troughs (Figure 21c). They currently have the lowest local elevation, some close to the elevation of TIS-1. The previous highest elevation of the NPLD, near 270°E has received relatively less accumulation since trough onset.

4.4. Interpacket Material

Using SHARAD, *Phillips et al.* [2008] observed packets of bright reflectors (200–500 m thick) separated by sequences of dim reflectors and speculated about the contents of each packet's material and potential climate signals imbedded within (Figures 3 of that paper and 3 of *Putzig et al.* [2009]).

In this survey we have detected previously unidentified outcrops of interpacket material at the surface in Regions 2 and 3. Figure 13b exhibits ~400 m of outcropped interpacket material just south and down slope of the central promontory, between a′ and a″. On the surface, the exposed material is highly layered and of medium to low albedo. Another exposure of interpacket material is found at 227°E, 86.5°N (Figure 3c). Dim reflectors reach the surface in the lowest 150 m of this trough. For both examples, there is no discernable difference in optical data to suggest a cause of the different radar properties. Interpacked material is exposed in other locations (Figures 10b, 11b, and 12b, Region 2, and Figure 18b).

5. Discussion

5.1. Comparison of the Regions

Our interpretations of the NPLD troughs agree with the interpretations of *Howard et al.* [1982] to varying degrees and conform to the characteristics described by the cyclic step model [*Smith et al.*, 2013]. Even though the observations agree in general, troughs are not all the same, and we delineate several distinct regions due to surface and subsurface characteristics.

In Region 1, where troughs are relatively simple, layers are nearly always exposed on the trough high sides, while low sides exhibit banded terrain (Figure 2e). In the subsurface, radar detects layer thinning near the high-side surface and thickening on the low side (Figure 4). Asymmetric accumulation, as implied by these observations, signifies material transport and trough migration. These troughs are best represented by the hypothetical cross section in Figure 5a.

Variety is detected in Region 1. The most prominent examples are the "V shapes" observed by *Smith and Holt* [2010] (Figure 9b). These structures are the result of layers onlapping a former central step or promontory (demonstrated via cartoon in Figure 5d). Rapid migration caused the high side to retreat faster at this elevation, leaving a step and decrease of TMP slope. Subsequent deposition outpaced migration, with associated TMP slope increase.

Region 2 troughs reside north and west of Chasma Boreale. Several characteristics separate these troughs from those in Region 1. Region 2 has a higher regional slope (0.27° versus 0.14°), the troughs are significantly deeper (up to 1 km versus ~400 m) [*Pathare and Paige*, 2005], and they have compound (W-shaped) cross sections. The combination of depth and shape causes these troughs to expose many more layers on the high side than Region 1 troughs. While it is clear that the W-shaped troughs were originally erosive, they exhibit draping low-side reflectors, evidence for migration (Figure 11b).

Region 3 is more diverse than either of Regions 1 or 2. As discussed above, low-latitude troughs share compound morphologies with Region 2. At higher latitudes, abundant undulations are observed (Figure 1) along with extensive stratigraphic records (Figure 14b). Simple troughs are found nearby (as in Figure 3b). Spatially, this region is very large, explaining some of the diversity.

Undulations are hypothesized to be similar to megadunes in Antarctica [*Herny et al*., 2014] which form in a similar way to sedimentary antidunes, resulting from katabatic flow [*Dadic et al*., 2013]. Antidunes form when the wind flow has Froude numbers approximately 0.9–1.2 [*Kennedy*, 1961; *Hand*, 1969, 1974; *Hand et al*., 1972], lower than the range of 1.7–5 for cyclic step (trough) formation [*Kostic et al*., 2010; *Smith et al*., 2013]. The parameters that most easily explain a change in Froude number for the NPLD are flow depth and velocity. Based on this argument, we find it likely that Region 3 experienced slower winds than in other regions (at least until the uppermost ~100 m were deposited).

Other evidence supports the interpretation of reduced wind speed for Region 3. Figure 3b demonstrates migration of a simple trough. When compared to troughs at the same latitude in Region 1 (Figure 2b), the trough is deeper and has reduced layer-thickness variations (cf. Figures 5a and 5b). Considering that insolation is the same between troughs at this latitude and deposition changes very little across each trough (until the winds move the material), a likely cause of this trough shape is reduced transport from slower winds. Region 3 troughs have migrated less than those of Region 1 (27 km versus ~90 km), another indication of reduced winds.

One question remains: the slope on which Region 3 troughs formed is steeper than in Region 1 (Table 1). Katabatic winds generally accelerate more on steeper slopes, so why is geomorphic evidence for weaker winds present? Perhaps the wind regime in Region 3 is more variable than in other regions, or larger-scale atmospheric properties may have been in effect. Modeling may provide an answer.

SHARAD returns are dominated by clutter in Region 4, making interpretation difficult. Observations nearest to the pole (and to Region 1) offer the best views of trough migration, in the form of sloping layers that vary in thickness. The offset of R29 at intersections with TMPs indicates that these troughs are some of the oldest on the NPLD (Figure 15). Little more can be determined from these observations.

Region 5 troughs are younger than those in the other regions. These troughs formed on an eroded surface, TIS-2, coinciding with R17, some 600 m higher than TIS-1. The reason for late-onset troughs in Region 5 may be simple. Prior to the erosion of TIS-2, the surface slopes in Region 5 were unfavorable for strong katabatic winds. A large paleochasma dominated this region at that time [*Holt et al*., 2010], and regional slopes oriented toward the pole, impeding katabatic flow (Figures 10, 16, and 21). After infill of the chasma, Regions 5 and perhaps 7 experienced large-scale erosion, corresponding to Gemini Scopuli. This erosion provided much steeper, equator-facing surface slopes, favorable for katabatic jumps to form.

Another plausible explanation is that atmospheric conditions changed at the time of erosion, finally allowing katabatic jumps to form. Evidence for concurrent trough migration throughout other regions sheds doubt on this hypothesis, and we prefer the favorable slope interpretation. Troughs may have existed at the margin of Region 5 prior to TIS-2 erosion, but any record would have been lost.

Troughs migrate upwind, not necessarily upslope. This is evident when one considers the wind direction (mapped by *Howard* [2000] and modeled by *Spiga et al*. [2011]), which is dominantly steered by the Coriolis force when relief is low. Region 5 troughs between the main lobe and Gemina Lingula have an atypical structure (Figure 19). Initially, the troughs formed parallel to the strike of TIS-2, but as wind acted on them from another direction, they migrated subparallel to TIS-2 erosion, resulting in a rotated appearance.

Region 6 troughs exemplify the radar characteristics of conventional troughs, but they are unique on the NPLD: they migrated away from the pole and are buried beneath ~125 m. Except for minor undulations (~10 m of relief), Region 6 is one of the smoothest locations on the NPLD (Figure 21). Those undulations agree with observed wind streaks [*Howard*, 2000] and modeling [*Spiga et al*., 2011] that the present winds come from the east rather than the south and imply that a previous wind regime was responsible for creating the troughs.

Region 7 corresponds to Gemina Lingula. We subdivide it into two groups. Region 7a corresponds to the western section of Gemini Scopuli. Troughs there orient more to the west than troughs in Regions 1–5 due to the source of winds being at the high point of Gemina Lingula [*Spiga et al.*, 2011]. Often possessing bedrock bottoms, marginal troughs do not preserve lower stratigraphy (Figure 9). Reflectors on either side of the TMP show asymmetric accumulation associated with transport. Atypically, low-side layers on the marginal scarps/troughs tilt toward the Gemina Lingula high point. Despite the unique qualities, evidence supports the interpretation of migration.

In Region 7b, on the north side of Gemina Lingula, we observe minor troughs (Figures 9 and 14d). These troughs are much smaller in cross section than troughs from other regions, and only slight deflections in the radar indicate their migration path. One such minor trough has migrated downwind (Figure 9c, left).

5.2. Relative Ages of Troughs

With SHARAD, we can determine the relative ages of troughs. The oldest troughs on the NPLD formed prior to deposition of R29 in Regions 1 and 4 (Figures 9 and 15). Afterward, we find evidence for lateral growth (especially eastward in Region 1 (Figure 8)). The exact stratigraphic level of initiation for each trough is not easily detected in Regions 2 and 3, but the troughs initiated shortly after the deposition of reflector R29, later than in Region 1 (Figure 3). Outside of Regions 5 and 7, most of the troughs on the NPLD had completed formation prior to R25.

We call these Generation 1 troughs. The increase in number and extent of troughs tells of initiation that was more gradual than punctuated. The entire process took place during the deposition of ~600 m ice from ~1100 m to ~500 m beneath the current surface. Prior to ~1100 beneath the current surface, no evidence of trough formation is found.

Instead of a single onset for Region 1 troughs, as previously hypothesized [*Smith and Holt*, 2010], Generation 1 troughs formed locally as conditions, such as increased regional slope or stronger winds, became favorable. The sole requirement of trough formation is that katabatic jumps form. Thus, the conditions for katabatic jumps became more widespread as the NPLD developed.

Region 5 troughs initiated much later than those in other regions, postdating the removal of significant amounts of material near Gemini Scopuli. We call these Generation 2 troughs. Unlike Generation 1, onset was punctuated, happening all at the same stratigraphic level.

The relative age of Region 7a troughs is more difficult to determine because of several factors. However, context provides necessary clues. Neighboring buried troughs in Region 6 formed near TIS-1. It is unlikely that the marginal, northeastward migrating troughs of Region 7a formed at the same time as the buried, southward migrating ones of Region 6. More probable is that Region 7a troughs share a common initiation period with Region 5 and TIS-2. This later date is consistent with geologic interpretations that Gemini Scopuli (encompassing Regions 5 and 7) is a unique region [*Tanaka and Fortezzo*, 2012].

5.3. Wavelength Dependence on Regional Slope

Troughs spacing is variable across the NPLD [*Pathare and Paige*, 2005], exemplified in Regions 1 and 5, where troughs are spaced by 40–50 and 20–30 km, respectively. Wavelength depends on the initial spacing of katabatic jumps because katabatic winds accelerate more quickly on a steeper slope, and jumps form closer together. Thus, the trough wavelength should be inversely related to the slopes on which they initiated [*Kostic et al.*, 2010; *Smith et al.*, 2013]. We find that both the initiation slope and characteristic wavelength of each region are not uniform throughout. Nevertheless, there is a good correlation between increasing slope and decreasing wavelength (Figure 22).

5.4. Variation in Migration

With a complete survey, it is possible to compare the different styles of migration detected, and we find evidence for regional- and smaller-scale variabilities. An example of the smaller-scale variability is the changing TMP slope within a single trough that indicates migration rates were not constant through time (Figure 5c).

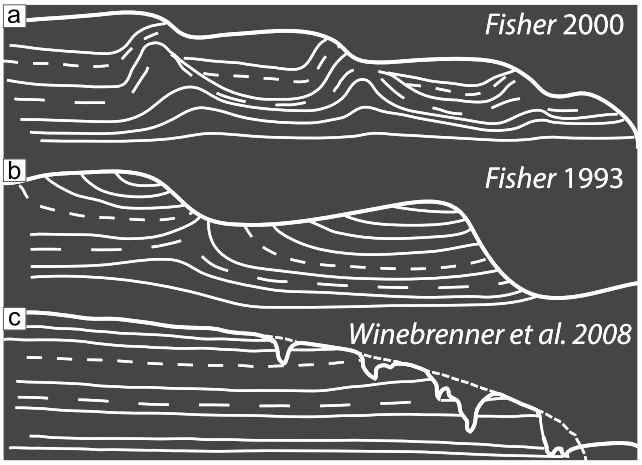

Figure 23. Cartoon depictions of predicted stratigraphy for different ice flow scenarios. (a and b) Two predicted stratigraphies for troughs existing during flow (modified from *Fisher* [1993, 2000]). These two cases predict that layers will rise beneath the troughs due to reduced overburden. (c) Trough formation postflow modified from *Winebrenner et al.* [2008]. Troughs in Gemina Lingula are incised, leaving layers that record former flow exposed on both the high and low sides, contrary to observations (Figures 9d and 20). None of these scenarios are found in our survey.

On a larger scale, Regions 1 and 6 troughs have the greatest asymmetry in accumulation on either side of a trough (Figures 2b and 4). This is a direct result of a relatively high proportion of wind transport (Figure 5a). In Region 3, where evidence supports lower intensity winds, asymmetry is present but small in comparison (Figures 3 and 5b). A drastic increase in TMP slope in Region 5 provides evidence for increased deposition relative to migration (Figures 5c and 17c). In this unique case, the TMP slope associated with a trough at 16°E, 82.5°N increases from 0.92° to 12.4°, the highest measured on the NPLD.

There are other, more complicated styles of migration observed on the NPLD. *Smith and Holt* [2010] detected anomalous "V" shaped stratigraphy at various troughs on the NPLD. We interpret the V-shaped reflectors to be the result of deposition over a central promontory or step (Figure 5d), and we find this feature in several regions, including Region 1 (Figure 9), Region 2 (Figure 10b), and Region 3 (Figure 11d). In some places, promontories are currently undergoing processes that may later form V-shaped anomalies.

5.5. Troughs and Ice Flow

Besides wind transport, flowing ice has been postulated to explain what we see related to troughs, undulations, and large-scale NPLD morphologies [*Fisher*, 1993; *Pathare and Paige*, 2005; *Winebrenner et al*., 2008]. Ice sheet modeling can accommodate the troughs in one of two ways: that the troughs existed during flow and were modified by it, or that the troughs formed after flow ceased. These models are predictive and testable. *Fisher* [1993, 2000] made the case for an "accublation" model of sublimation and accumulation, allowing for the troughs to exist and remain open during flow. In this model, layers beneath the spiral troughs would flow upward due to reduced overburden (Figure 23a). Our survey finds no stratigraphy on the NPLD matching this prediction.

A second hypothesis suggested that trough topography would relax over time, eventually closing and becoming smooth [*Pathare and Paige*, 2005]. Our survey reveals that the oldest troughs have existed throughout 1 km of deposition, approximately one half of the accumulation of the entire NPLD (Figure 9b). Additionally, Region 1 troughs have grown in amplitude and cross-sectional width, have increased in number, and have migrated as many as 90 km. While we cannot rule out trough relaxation, it must occur on a timescale much slower than the processes controlling trough migration.

In a study of NPLD topography, *Winebrenner et al*. [2008] suggested that Gemina Lingula flowed and reached steady state ice sheet morphology prior to trough formation (Figure 23c). Their balanced ice sheet hypothesis requires the surface to be a smooth dome during flow (or an upwelling beneath troughs would occur as predicted by *Fisher* [1993, 2000]). However, we observe trough onset in Gemina Lingula well below the current surface (Figures 9d and 15d). The additional discovery of buried troughs in Region 6 (Figure 20) cannot be reconciled with the assumption of trough incision postflow unless flow occurred prior to deposition of R29, some 700 m beneath the current surface.

Because of the discrepancies of internal stratigraphy predicted by ice flow models and those observed in both this study and that of *Karlsson et al*. [2011], we posit that there was no significant role for ice flow in the evolution of the troughs on the NPLD.

6. Conclusions

Spiral troughs across the NLD are both fundamentally similar and richly diverse. Every trough exhibits common features, including layered high sides, banded low sides, asymmetric slopes, and albedo variations. Beneath the surface, SHARAD detects asymmetric accumulation patterns and migration paths at all troughs where observations can be made. Even though they can all be described similarly, regional and local differences make each unique. Troughs vary based on local and regional surface slopes, wavelengths, trough depths, relative age, presence of topographic undulations, presence of central promontories, and trough floors that reach bedrock. To better classify this diversity, we have divided the NPLD into eight regions, separating troughs based on these differences.

The troughs did not all form at the same time, and they can be divided into two generations. Generation 1 troughs reside in Regions 1–4 and 6. Radar evidence supports a gradual increase in number and longitudinal extent of Generation 1 troughs during deposition of more than 600 m, starting about 1100 m beneath the current surface. Generation 2 troughs are found in Regions 5 and probably in 7a, both corresponding to Gemini Scopuli. The onset of troughs in Region 5 was relatively rapid after widespread erosion removed a significant amount of material.

Troughs are not static features, and they evolve both independently based on local processes and as a group when considered by region. This evolution plays out over million-year timescales. Some of the changes the troughs have undergone include increase in number, burial, evolution from compound to simple, or merging.

As described by *Smith et al*. [2013], three common processes are sufficient to explain all of the features and varieties discussed in this paper: transport, insolation, and deposition. These processes are present in every region of the NPLD, but they are not uniform. Winds have variable strengths based on local and regional conditions. For example, Region 3 troughs, while at the same latitude as those in Region 1, are comparatively steeper and have reduced asymmetry patterns. They are also accompanied by prominent topographic undulations. Each of those qualities is evidence for reduced wind intensity in Region 3. Region 5 and 7 troughs are steeper than those of other regions. Even with all of the observed variation, no evidence is present to support interpretations of other processes controlling trough evolution such as ice flow, volcanism, or tectonics.

Multiple conclusions may be made from our survey: (1) trough spacing has an inverse relationship to regional initiation slope; (2) Region 5 and 7a troughs formed immediately after a large-scale erosion, in contrast to other regions, where troughs initiated and grew during a period of ongoing deposition; (3) physical properties and processes important to trough evolution include trough strike, albedo, high- and low-side slopes, depth, and wind patterns. These properties influence the winds and insolation associated with trough evolution and are themselves modified by them.

Appendix A: Color Codes to Reflectors

A summary of common reflector names and color codes used throughout this paper (Table A1).

Table A1. Reflectors Discussed in This Paper

Reflector	Color	Other Name	Description	Location
R17	Green	TIS-2	Corresponds exactly to initiation of Generation 2 troughs	Shown primarily in Region 5
R25	Light Blue	TIS-1	Corresponds roughly to initiation of Generation 1 troughs	Shown throughout the NPLD
R29	Red			Shown throughout the NPLD

Acknowledgments
This work was supported by NASA ESSF Fellowship NNX10AT24H, NASA MDAP grant NNX10AO26G, the MRO SHARAD team, and the Jackson School of Geosciences. Data used in this work are available from the NASA Planetary Data System or from the Colorado SHARAD Radar Processing System (CO-SHARPS; contact co-sharps@ops.boulder.swri.edu for more information). We are very grateful to Than Putzig for constructive comments.

References

Blasius, K. R., J. A. Cutts, and A. D. Howard (1982), Topography and stratigraphy of Martian polar layered deposits, *Icarus*, *50*(2–3), 140–160.
Brothers, T. C., J. W. Holt, and A. Spiga (2013), Orbital radar, imagery, and atmospheric modeling reveal an aeolian origin for Abalos Mensa, Mars, *Geophys. Res. Lett.*, *40*, 1334–1339, doi:10.1002/grl.50293.
Byrne, S. (2009), The polar deposits of Mars, *Annu. Rev. Earth Planet. Sci.*, *37*(1), 535–560, doi:10.1146/annurev.earth.031208.100101.
Campbell, B. A., N. E. Putzig, L. M. Carter, and R. J. Phillips (2011), Autofocus correction of phase distortion effects on SHARAD echoes, *Geosci. Remote Sens. Lett.*, *8*(5), 939–942, doi:10.1109/LGRS.2011.2143692.
Christian, S., J. W. Holt, S. Byrne, and K. E. Fishbaugh (2013), Integrating radar stratigraphy with high resolution visible stratigraphy of the north polar layered deposits, Mars, *Icarus*, *226*, 1241–1251.
Cutts, J. A. (1973), Nature and origin of layered deposits of the Martian polar regions, *J. Geophys. Res.*, *78*(20), 4231–4249, doi:10.1029/JB078i020p04231.
Cutts, J. A., and B. H. Lewis (1982), Models of climate cycles recorded in Martian polar layered deposits, *Icarus*, *50*(2–3), 216–244.
Cutts, J. A., K. Blasius, and W. Roberts (1979), Evolution of Martian polar landscapes: Interplay of long-term variations in perennial ice cover and dust storm intensity, *J. Geophys. Res.*, *84*(B6), 2975–2994, doi:10.1029/JB084iB06p02975.
Dadic, R., R. Mott, H. J. Horgan, and M. Lehning (2013), Observations, theory, and modeling of the differential accumulation of Antarctic megadunes, *J. Geophys. Res. Earth Surf.*, *118*, 2343–2353, doi:10.1002/2013JF002844.
Fishbaugh, K. E., and C. S. Hvidberg (2006), Martian north polar layered deposits stratigraphy: Implications for accumulation rates and flow, *J. Geophys. Res.*, *111*, E06012, doi:10.1029/2005JE002571.
Fishbaugh, K. E., S. Byrne, K. E. Herkenhoff, R. L. Kirk, C. Fortezzo, P. S. Russell, and A. McEwen (2010), Evaluating the meaning of "layer" in the Martian north polar layered deposits and the impact on the climate connection, *Icarus*, *205*, 269–282, doi:10.1016/j.icarus.2009.04.011.
Fisher, D. A. (1993), If Martian ice caps flow: Ablation mechanisms and appearance, *Icarus*, *105*(2), 501–511.
Fisher, D. A. (2000), Internal layers in an "Accublation" Ice Cap: A test for flow, *Icarus*, *144*(2), 289–294.
Grima, C., W. Kofman, J. Mouginot, R. J. Phillips, A. Hérique, D. Biccari, R. Seu, and M. Cutigni (2009), North polar deposits of Mars: Extreme purity of the water ice, *Geophys. Res. Lett.*, *36*, L03203, doi:10.1029/2008GL036326.
Hand, B. M. (1969), Antidunes as trochoidal waves, *J. Sediment. Res.*, *39*(4), 1302–1309, doi:10.1306/74D71E15-2B21-11D7-8648000102C1865D.
Hand, B. M. (1974), Supercritical flow in density currents, *J. Sediment. Res.*, *44*(3), 637–648, doi:10.1306/74D72AB3-2B21-11D7-8648000102C1865D.
Hand, B. M., G. V. Middleton, and K. Skipper (1972), Antidune cross-stratification in a turbidite sequence, Cloridome Formation, Gaspé, Quebec, *Sedimentology*, *18*(1–2), 135–138, doi:10.1111/j.1365-3091.1972.tb00009.x.
Head, J. W., J. F. Mustard, M. A. Kreslavsky, R. E. Milliken, and D. R. Marchant (2003), Recent ice ages on Mars, *Nature*, *426*, 797–802.
Herny, C., M. Masse, O. Bourgeois, S. Carpy, S. Le Mouelic, T. Appere, I. B. Smith, A. Spiga, and S. Rodriguez (2014), Sedimentation waves on the Martian North Polar Cap: Analogy with megadunes in Antarctica, *Earth Planet. Sci. Lett.*, doi:10.1016/j.epsl.2014.06.033.
Holt, J. W., M. E. Peters, S. D. Kempf, D. L. Morse, and D. D. Blankenship (2006), Echo source discrimination in single-pass airborne radar sounding data from the Dry Valleys, Antarctica: Implications for orbital sounding of Mars, *J. Geophys. Res.*, *111*, E06S24, doi:10.1029/2005JE002525.
Holt, J. W., A. Safaeinili, J. J. Plaut, J. W. Head, R. J. Phillips, R. Seu, S. D. Kempf, P. Choudhary, D. A. Young, and N. E. Putzig (2008), Radar sounding evidence for buried glaciers in the southern mid-latitudes of Mars, *Science*, *322*(5905), 1235.
Holt, J. W., K. E. Fishbaugh, S. Byrne, S. Christian, K. Tanaka, P. S. Russell, K. E. Herkenhoff, A. Safaeinili, N. E. Putzig, and R. J. Phillips (2010), The construction of Chasma Boreale on Mars, *Nature*, *465*(7297), 446–449.
Howard, A. D. (2000), The role of eolian processes in forming surface features of the Martian polar layered deposits, *Icarus*, *144*(2), 267–288.
Howard, A. D., J. A. Cutts, and K. R. Blasius (1982), Stratigraphic relationships within Martian polar cap deposits, *Icarus*, *50*(2–3), 161–215.
Hvidberg, C. S., K. E. Fishbaugh, M. Winstrup, A. Svensson, S. Byrne, and K. E. Herkenhoff (2012), Reading the climate record of the Martian polar layered deposits, *Icarus*, *221*(1), 405–419, doi:10.1016/j.icarus.2012.08.009.
Karlsson, N. B., J. W. Holt, and R. C. A. Hindmarsh (2011), Testing for flow in the north polar layered deposits of Mars using radar stratigraphy and a simple 3D ice-flow model, *Geophys. Res. Lett.*, *38*, L24204, doi:10.1029/2011GL049630.
Kennedy, J. F. (1961), *Stationary Waves and Antidunes in Alluvial Channels*, Calif. Inst. of Technol., Pasadena.
Kolb, E. J., and K. L. Tanaka (2001), Geologic history of the polar regions of Mars based on Mars global surveyor data: II. Amazonian period, *Icarus*, *154*(1), 22–39.
Kostic, S., O. Sequeiros, B. Spinewine, and G. Parker (2010), Cyclic steps: A phenomenon of supercritical shallow flow from the high mountains to the bottom of the ocean, *J. Hydro-environ. Res.*, *3*(4), 167–172.
Laskar, J., B. Levrard, and J. F. Mustard (2002), Orbital forcing of the Martian polar layered deposits, *Nature*, *419*(6905), 375–377.
Levrard, B., F. Forget, F. Montmessin, and J. Laskar (2007), Recent formation and evolution of northern Martian polar layered deposits as inferred from a global climate model, *J. Geophys. Res.*, *112*, E06012, doi:10.1029/2006JE002772.
Milkovich, S. M., and J. W. Head (2005), North polar cap of Mars: Polar layered deposit characterization and identification of a fundamental climate signal, *J. Geophys. Res.*, *110*, E01005, doi:10.1029/2004JE002349.
Milkovich, S. M., J. J. Plaut, A. Safaeinili, G. Picardi, R. Seu, and R. J. Phillips (2009), Stratigraphy of Promethei Lingula, south polar layered deposits, Mars, in radar and imaging data sets, *J. Geophys. Res.*, *114*, E03002, doi:10.1029/2008JE003162.
Murray, B. C., L. A. Soderblom, J. A. Cutts, R. P. Sharp, D. J. Milton, and R. B. Leighton (1972), Geological framework of the south polar region of Mars, *Icarus*, *17*(2), 328–345.
Ng, F. S. L., and M. T. Zuber (2006), Patterning instability on the Mars polar ice caps, *J. Geophys. Res.*, *111*, E02005, doi:10.1029/2005JE002533.
Pathare, A. V., and D. A. Paige (2005), The effects of Martian orbital variations upon the sublimation and relaxation of north polar troughs and scarps, *Icarus*, *174*(2), 419–443.
Pelletier, J. D. (2004), How do spiral troughs form on Mars?, *Geology*, *32*(4), 365–367.
Phillips, R. J., et al. (2008), Mars north polar deposits: Stratigraphy, age, and geodynamical response, *Science*, *320*(5880), 1182.
Picardi, G., J. J. Plaut, D. Biccari, O. Bombaci, D. Calabrese, M. Cartacci, A. Cicchetti, S. M. Clifford, P. Edenhofer, and W. M. Farrell (2005), Radar soundings of the subsurface of Mars, *Science*, *310*(5756), 1925–1928.
Putzig, N. E., R. J. Phillips, B. A. Campbell, J. W. Holt, J. J. Plaut, L. M. Carter, A. F. Egan, F. Bernardini, A. Safaeinili, and R. Seu (2009), Subsurface structure of Planum Boreum from Mars Reconnaissance Orbiter shallow radar soundings, *Icarus*, *204*(2), 443–457.
Rodriguez, J. A. P., and K. L. Tanaka (2011), Evidence for in-situ trough erosion in Planum Boreum, Mars, Fifth International Conference on Mars Polar Science and Exploration, 1323, Abstract 6015.
Seu, R., et al. (2007), SHARAD sounding radar on the Mars Reconnaissance Orbiter, *J. Geophys. Res.*, *112*, E05S05, doi:10.1029/2006JE002745.
Smith, D. E., et al. (2001), Mars Orbiter Laser Altimeter: Experiment summary after the first year of global mapping of Mars, *J. Geophys. Res.*, *106*(E10), 23,689–23,722, doi:10.1029/2000JE001364.

Smith, I. B., and J. W. Holt (2010), Onset and migration of spiral troughs on Mars revealed by orbital radar, *Nature*, *465*(7297), 450–453, doi:10.1038/nature09049.

Smith, I. B., J. W. Holt, A. Spiga, A. D. Howard, and G. Parker (2013), The spiral troughs of Mars as cyclic steps, *J. Geophys. Res. Planets*, *118*, 1835–1857, doi:10.1002/jgre.20142.

Smith, I. B., A. Spiga, and J. W. Holt (2014), Aeolian processes as drivers of landform evolution at the south pole of Mars, *Geomorphology*, doi:10.1016/j.geomorph.2014.08.026.

Spiga, A., F. Forget, J. B. Madeleine, L. Montabone, S. R. Lewis, and E. Millour (2011), The impact of Martian mesoscale winds on surface temperature and on the determination of thermal inertia, *Icarus*, *212*, 504–519.

Squyres, S. W. (1979), The evolution of dust deposits in the Martian north polar region, *Icarus*, *40*(2), 244–261.

Tanaka, K. L., and C. M. Fortezzo (2012), Geologic map of the north polar region of Mars: U.S. Geological Survey Scientific Investigations Map 3177.

Tanaka, K. L., J. A. P. Rodriguez, J. A. Skinner, M. C. Bourke, C. M. Fortezzo, K. E. Herkenhoff, E. J. Kolb, and C. H. Okubo (2008), North polar region of Mars: Advances in stratigraphy, structure, and erosional modification, *Icarus*, *196*(2), 318–358.

Weijermars, R. (1986), The polar spirals of Mars may be due to glacier surges deflected by Coriolis forces, *Earth Planet. Sci. Lett.*, *76*(3–4), 227–240.

Winebrenner, D. P., M. R. Koutnik, E. D. Waddington, A. V. Pathare, B. C. Murray, S. Byrne, and J. L. Bamber (2008), Evidence for ice flow prior to trough formation in the Martian north polar layered deposits, *Icarus*, *195*(1), 90–105.

Zeng, Z., N. E. Putzig, H. Xie, S. J. Birnbaum, S. F. Ackely, and L. Liu (2008), Evidence of fractures in NPLD and their significance to the formation of Martian polar spiral troughs, Anon. 39th LPSC, LPI, League City, Abstract 2179.